

Article

Dynamics of Vortex Structures: From Planets to Black Hole Accretion Disks

Elizabeth P. Tito¹  and Vadim I. Pavlov^{1,2,*} ¹ Scientific Advisory Group, Pasadena, CA 91125, USA² Laboratoire de Mécanique des Fluides de Lille–Kampé de Fériet–LMFL–UMR 9014 CNRS ONERA, Arts et Métiers Institute of Technology, Centrale Lille, University of Lille, F-59000 Lille, France

* Correspondence: vadim.pavlov@univ-lille.fr

Abstract: Thermo-vortices (bright spots, blobs, swirls) in cosmic fluids (planetary atmospheres, or even black hole accretion disks) are sometimes observed as clustered into quasi-symmetrical quasi-stationary groups but conceptualized in models as autonomous items. We demonstrate—using the (analytical) Sharp Boundaries Evolution Method and a generic model of a thermo-vortical field in a rotating “thin” fluid layer in a spacetime that may be curved or flat—that these thermo-vortices may be not independent but represent interlinked parts of a single, coherent, multi-petal macro-structure. This alternative conceptualization may influence the designs of numerical models and image-reconstruction methods.

Keywords: vortex dynamics; relativistic dynamics; fluid dynamics; hot spots; thermo-vortices; large-scale structures; black hole accretion disk; planetary atmosphere; planetary ocean; methods: analytical

1. Introduction

Recently, a highly complex analysis of observations of the black hole Sagittarius A* (Sgr A*) yielded an impressive image (see Figure 1, panel A) that suggests the possible presence of three bright spots within its structure outside the shadow of a black hole (see Refs. [1–6]). Visually, this phenomenon is resemblant of the formations already observed in the atmospheres of planets (also shown in Figure 1, panels B–D). Indeed, regular in shape, long-lasting vortices and multi-vortex structures appear frequently in nature; some well-known examples are the Antarctic Polar Vortex, oceanic vortices, cyclones and anti-cyclones in atmospheres, cyclone storms on Jupiter poles, and analogous vortex structures in the atmospheres of outer planets. If further observational studies confirm that the bright spots in Figure 1A are not artifacts of the image-reconstruction algorithm but are indeed physical in nature (apparently associated with temperature anomalies/emissions in localized areas), then the list of known cosmic environments with multi-vortex structures would be expanded to include black hole accretion disk flows.

All vortex structures are naturally studied using frameworks and models that seem most appropriate for their native environments. Typically, however, the individual vortices are conceptualized as stand-alone items, sometimes interacting, sometimes not.

In this paper—while contemplating the image presented in Figure 1A and its visually bright spots (although the only significant real feature in the image is the shadow and its diameter, the non-uniformity of the brightness along the ring is not very significant and is subject to processing/reconstruction methods)—we analytically demonstrate that such spots may exist and represent *connected “petals” of a single multi-petal thermo-vortical macro-structure*. Within such a structure, the vorticity of the “hydrodynamic” (i.e., collective) flow is interlinked with the temperature field of the medium. This vorticity, a Lagrangian characteristic of the hydrodynamic flow, is transported by the flow, thus creating spots with an elevated temperature.

**Citation:** Tito, E.P.; Pavlov, V.I.Dynamics of Vortex Structures: From Planets to Black Hole Accretion Disks. *Dynamics* **2024**, *4*, 357–393. <https://doi.org/10.3390/dynamics4020021>

Academic Editor: Christos Volos

Received: 1 April 2024

Revised: 7 May 2024

Accepted: 8 May 2024

Published: 13 May 2024



Copyright: © 2024 by the authors. Licensee MDPI, Basel, Switzerland. This article is an open access article distributed under the terms and conditions of the Creative Commons Attribution (CC BY) license (<https://creativecommons.org/licenses/by/4.0/>).

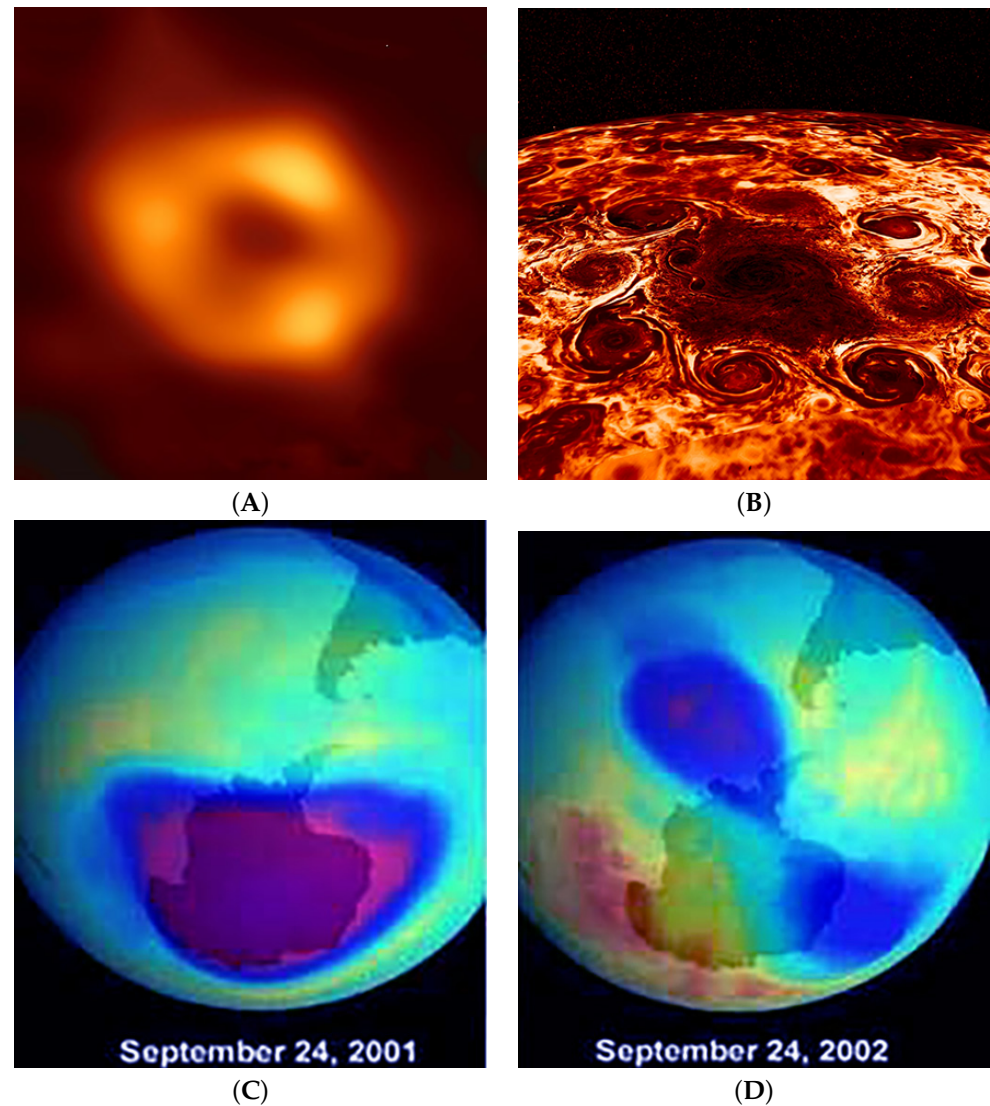


Figure 1. First Row, Left Panel (A): Composite image of the black hole Sgr A* derived from radio (1.3 mm) data collected by the Event Horizon Telescope (EHT) Collaboration [1]. **First Row, Right Panel (B):** Multiple cyclones on Jupiter’s North Pole [7]. **Second Row, Left Panel (C):** The Antarctic Ozone Hole in Earth’s stratosphere; the vortex is quasi-circular on 24 September 2001. **Second Row, Right Panel (D):** The vortex evolved into a two-petal structure by 24 September 2002. Credit: NASA’s Earth Observatory [8].

The awareness of the existence of two interpretations of the structure and the linkage of thermo-vortices is important. The initial conceptualization—whether the thermo-vortices are treated from the start as stand-alone items or as inextricable parts of one macro-structure—may meaningfully influence the numerical models and image-reconstruction methods.

In our model, we make the following assumptions and impose the following restrictions: the flow of the disk fluid is assumed to be large-scale (the Reynolds number or its analogue is large, i.e., viscous effects are small and may be neglected); the flow is slow (relative to the sound speed); and the assumption of medium incompressibility is acceptable. To simplify the mathematical complexity of analytic solutions, our model considers the “thin”-layer case: (1) it is assumed that the accretion disk is relatively thin, i.e., the characteristic size of the structure is assumed to be significantly larger than the characteristic thickness of the disk (layer) at the location at which the structure is localized; (2) the motion of the medium is assumed to be quasi-two-dimensional, i.e., the component of the collective flow velocity in the direction perpendicular to the disk plane is suppressed or significantly

smaller in magnitude than the characteristic flow velocity in the disk plane (in this context, a “thick” system may also, in principle, be described using the two-dimensional treatment if a vorticity patch is broken into columnar sub-patches, as in Refs. [9,10]); (3) the temperature decreases towards the center of the disk due to the assumption that the heating of the disk mainly occurs not from the hot central body but from the periphery where the capture and destruction of captured bodies occurs due to the tidal effect.

The medium (disk layer) in our model is presumed to rotate. Vorticity is non-zero where there is velocity shear. We describe the “average” vorticity, representative of some “band” within the disk, using the symbol ω . (Obviously, this vorticity ω is not the same as the spin of the central body or the characteristic angular velocity Ω of the disk’s rotation.) When Ω is “sufficiently” high, the centrifugal effects (in the rotating frame) become prominent in the leading terms, and even dominate the gravitational effect of attraction to the central body.

To avoid any confusion, for the modelers accustomed to working with *trajectories* for *particles*, let us emphasize that we work with the *field*, not with individual particles (or their trajectories or orbits). Perhaps what may help the reader grasp this nuance better is the reminder that the velocity of the displacement of electrons in a usual house-wire is not the same thing as the speed of propagation of the electro-magnetic field perturbation along that same wire.

Additionally, we limit our consideration to the case when the magnetic field is weak and the plasma is non-relativistic. This means that in our treatment we neglect the effect of the magnetic field on the large-scale “hydrodynamics” of the flow, i.e., in the full tensor of the energy–momentum of the macroscopic “hydrodynamic” flow combined with the electromagnetic field, we neglect the magnetic part. However, this does not mean that this “weak” magnetic field has no impact on the electromagnetic radiation (for example, on the polarization of the synchrotron radiation). Indeed, as Ref. [11] indicates, EHT images in linear polarization have identified a coherent spiral pattern around the black hole, produced from ordered magnetic fields threading the emitting plasma.

Finally, our focus is on *steady-state* thermo-hydrodynamic structures. This is important to keep in mind for numerical modelers who typically initiate their models at time $t = 0$ (and may start, for example, with the spherical Bondi accretion) and allow their models to evolve towards some steady state (hoping to minimize accumulated errors along the way). In contrast, our steady-state is derived *analytically*; we jump straight to the model of a flattened rotating medium (disk, layer) and examine its quasi-stationary dynamics.

The paper is organized as follows: Section 2 explains the model, Section 3 presents the results, and Section 4 concludes with the discussion. Appendices A and B explain the details of calculations; Appendix C elaborates the accretion disk model.

The derived insights may be useful for analyses of environments ranging from accretion disks (in an approximation of curved spacetime) to planetary atmospheres (in an approximation of flat spacetime): the design of numerical models and image reconstruction methods may be influenced by how the steady-state of the media is conceptualized—as multiple (separate) quasi-localized vortices or as a single (integrated) multi-petal structure.

2. Model

We use the quasi-2D fluid dynamics model, which describes large-scale vorticial motions of a “thin” rotating disk in a mildly curved spacetime.

Coordinates and Notations: In the model, we use the coordinate system where $x \equiv x_1$ and $y \equiv x_2$ are the axes in the horizontal plane and z points vertically up. We employ the following notations: Φ is the potential of the force field; temperature $\theta \equiv \theta_0 + \tau_s + \tau$, where θ_0 is the (constant) baseline temperature of the disk, τ_s is the spatially inhomogeneous, axially symmetrical, time-independent part of the temperature distribution, and $\tau = \tau(t, x_j)$ is the temperature—a dynamical quantity related to the vortex structures in the fluid; v_i signifies the components of the velocity field \mathbf{v} ; ω_3 is the z -component of vorticity $[\nabla \times \mathbf{v}]$; and ϵ_{ijk} is the standard alternating tensor ($\epsilon_{123} = 1$, $\epsilon_{ijk} = 0$ when any two indices are

equal, $\epsilon_{ijk} = +1$ for any even number of permutations of indices from ϵ_{123} , and $\epsilon_{ijk} = -1$ for any odd number of permutations). Note also that $\epsilon_{3jk}\partial_j\tau_s\partial_k\Phi \equiv 0$ because both τ_s and Φ are axially symmetric. Furthermore, we assume that the band of the disk between r_1 and $r_2 > r_1$, where the vortex structure of interest is formed, is characterized by an approximately constant angular velocity $\Omega = (0, 0, \Omega)$.

“Thin” Disk: In the simplest model—in which the vortex structures are realized in a “thin” flat sheet with $h \ll L$, $V^2 \ll s^2 \ll c^2$, $Re \gg 1$ —the z -component of velocity, w , vanishes and may be dropped in all formulas (see Ref. [10], developing this particular model, or classical Refs. [12–14]). Here, h is the characteristic local thickness of the disk, which is slowly dependent on the radial coordinate; L is the characteristic spatial length over which the macroscopic flow characteristics change substantially; s is the so-called “isothermal sound speed”; V is the characteristic fluid velocity; c is the speed of light; dimensionless parameter Re is the Reynolds number (or its analogs) such that $Re \gg 1$.

The System of Equations: The set of equations for the z -component of vorticity ω_3 and for variations in temperature τ becomes:

$$\partial_j v_j = 0, \quad D_t \omega_3 = \beta \epsilon_{3jk} \partial_j \tau \partial_k \Phi, \quad D_t \tau = -v_i \partial_i \tau_s, \tag{1}$$

where indices $j, k = 1, 2$. Operator $D_t \equiv \partial_t + v^k \partial_k$ is the total derivative. The condition of incompressibility $div \mathbf{v} = 0$ does not mean that the density of the medium is constant. This condition simply means that the density evolves according to the equation $(\partial_t + v^l \partial_l) \rho = 0$. Taking $\rho = \rho_0 + (\partial \rho / \partial T)_p (T - T_0) + (\partial \rho / \partial p)_T (p - p_0) \simeq \rho_0 (1 - \beta (T - T_0))$, after some simple manipulation, the evolution equation for temperature perturbations takes the form of the third equation in Equation (1). For the equation of state, we will assume, in accordance with the assumption $div \mathbf{v} \rightarrow 0$, that the density essentially depends only on the temperature and not on the pressure. Thus, we write $\rho \simeq \rho_0 (1 - \beta (T - T_0))$, where subscript 0 denotes the reference values. The coefficient of thermal expansion $\beta = -\rho^{-1} (\partial \rho / \partial p)_T$ is presumed to be constant in the layer. Since quantity $\beta (T - T_0)$ is generally small (relative to 1), one may neglect the density variations and hence replace ρ with the constant value ρ_0 in all terms of the dynamic momentum equation except for the “buoyancy” term.

We will presume that a collective fluid motion forms in the system, for which the relationship between the flow velocity and temperature variation is given by

$$v_i = a \epsilon_{3ij} \partial_j \tau \equiv a \epsilon_{ij} \partial_j \tau. \tag{2}$$

Here, tensor ϵ_{ij} is the antisymmetric unit, second-order tensor, for which $\epsilon_{12} = -\epsilon_{21}$ and the diagonal components are zero; and a is some parameter assuring the correct dimension for the relationship between the considered quantities. In this case, vorticity $\omega_3 = -a \Delta \tau + 2\Omega_3$, where $\Delta = \partial_1^2 + \partial_2^2$. Then, notably, the presence (or absence) of the component with constant Ω_3 does not impact the core set of Equation (1).

As mentioned, the vortical field is intertwined with the thermal field. Thus, in addition to the set of Equation (1), any model must include equations for the temperature field. We set the ansatz for the temperature profile as $\theta \equiv \theta_0 + \tau_s + \tau$, where θ_0 is the (constant) baseline temperature of the disk, τ_s is the spatially inhomogeneous, axially symmetrical, time-independent part of the temperature distribution, and $\tau = \tau(t, x_j)$ is the temperature—a dynamical quantity related to the vortex structures in the fluid. We chose the stationary temperature deviation τ_s in a form that allows for a self-consistent analytical solution. This choice does not contradict experimental observations (see, for example, Ref. [15]). Therefore, we will model (using notation $r = |\mathbf{x}|$ and $\mathbf{x} = (x_1, x_2)$, and the Taylor series expansion) the background distribution of the time-independent temperature deviation τ_s in the simplest form:

$$\tau_s = \frac{\tau_1}{2} r^2, \quad \tau_1 > 0, \tag{3}$$

where τ_1 is the parameter characterizing the “rapidity” of the increase in the basal temperature of the medium as the distance r from the disk rotation axis grows. (Generally speaking, the question of what shape the temperature profile takes within a black hole’s accretion disk is an open one. Astronomical measurements remain challenging, despite significant progress. See, for example, Refs. [15,16].) When the leading contribution to potential Φ comes from the centrifugal effects, we can express $\Phi = -K^2|\mathbf{x}|^2 - (1/2)[\boldsymbol{\Omega}, \mathbf{x}]^2 \simeq -(1/2)[\boldsymbol{\Omega}, \mathbf{x}]^2$. Here, the square brackets denote the cross product of two vectors. Parameter K^2 is determined by the expression $K^2 = GM_{BH}/r^3 = c^2 r_g / (2r^3)$, where $K \sim r^{-3/2}$ is the so-called Kepler parameter (in the Newtonian approximation of gravity), which is interpreted as the angular velocity of a test particle on a circular orbit at distance r : G is the gravitational constant; c is the speed of light; M_{BH} is the black hole “mass”. Thus, when angular velocity $\boldsymbol{\Omega}$ is presumed to remain constant within the band of r where the thermo-vortical macro-structure forms, the set of the interlinked nonlinear evolution equations becomes:

$$a\partial_t\Delta\tau + a^2\epsilon_{ik}\partial_i\tau\partial_k\Delta\tau = \beta\Omega^2\epsilon_{ik}x_i\partial_k\tau, \tag{4}$$

$$\partial_t\tau + a\epsilon_{ik}\partial_i\tau\partial_k\tau = a\tau_1\epsilon_{ik}x_i\partial_k\tau, \tag{5}$$

where, obviously, quantity $v_k = a\epsilon_{ik}\partial_i\tau$ is the k -th component of the flow velocity.

Equations (4) and (5) have a transparent physical meaning. Their left sides describe the transport of dynamic (field) quantities: vorticity ($\sim\Delta\tau$) and temperature perturbation (τ). The right sides of these equations describe “sources” that generate the vortices and the temperature perturbations. In other words, the vortices are generated by the source described by the right part of Equation (4), which is effective (non-zero) only when there exists an inhomogeneous gravity-like force field $\Phi \sim \Omega^2$ with which temperature perturbation τ interacts via the equation of state (when compressibility $\beta \neq 0$), while the quantity $\Delta\tau$ —which characterizes the vortex field in the fluid—is transported by the self-induced flow (the left part of Equation (4)). On the other hand, in Equation (5), temperature perturbation τ is transported by the self-generated flow ($v_i \neq 0$); temperature perturbation $\tau(t, \mathbf{x})$ is generated by the source (the right part of Equation (5)), which is non-zero only when there exists a spatial- and time-independent temperature gradient (i.e., when $\tau_1 \neq 0$). The processes are interlinked because the “source” of one dynamic quantity depends on a complex combination of other dynamic quantities. Equations (4) and (5) show that when the stratification of temperature is absent ($\tau_1 = 0$) and there is no disk rotation ($\boldsymbol{\Omega} = 0$, i.e., centrifugal force is zero), then Equations (4) and (5) degenerate into the traditional equations for vortex evolution and transport in a two-dimensional ideal fluid. Comparing Equations (4) and (5), we conclude that both the first and second equations describe the evolution of the same physical entity. As follows from the definition of hydrodynamical velocity, the dimension of coefficient a is $[a] = \theta^{-1}L^2T^{-1} \equiv [temperature]^{-1} \times [length]^2 \times [time]^{-1}$.

Lagrangian Quantity (“Q-Vorticity”): By combining Equations (4) and (5), i.e., after multiplying the second equation by $\beta\Omega^2/a\tau_1$ and subtracting it from the first, we obtain:

$$(\partial_t + a\epsilon_{ik}\partial_i\tau\partial_k)(\Delta\tau - R^{-2}\tau) = 0. \tag{6}$$

Here, parameter $R^{-2} = a^{-2}(\beta/\tau_1)\Omega^2$. Its dimension is $(\theta^1L^{-2}T^1)^2 \times \theta^{-1} \times \theta^{-1}L^2 \times T^{-2} = L^{-2}$, showing that R is a space scale factor. If the question is posed to examine the evolution of the temperature field, then the nonlinear differential equation Equation (6) is solved numerically, specifying the initial distribution of the temperature field, as well as the spatial boundary conditions.

On the other hand, we may define a new quantity

$$q \equiv a(\Delta\tau - R^{-2}\tau), \tag{7}$$

which we will call “q-vorticity” because this quantity is linked to the streamfunction via definitions. This quantity is transported by the flow according to Equation (6), i.e., as

a Lagrangian quantity. Thus, the integral of any function of q in the xy -plane is always conserved.

Temperature: Temperature τ is found via the Green function representation. It is presented as follows:

$$\tau(\mathbf{x}, t) = \frac{1}{a} \int d\mathbf{x}' G(\mathbf{x}, \mathbf{x}') q(\mathbf{x}', t). \tag{8}$$

Here, the Green function satisfies the following equation:

$$(\Delta - R^{-2})G = \delta(\mathbf{x}, \mathbf{x}'), \tag{9}$$

where δ is the Dirac delta-function. The collective “hydrodynamical” velocity of the flow (orthogonal to the temperature gradient) is calculated using Equation (2).

Modeling Steady-State: So, what is the initial vorticity distribution $q(\mathbf{x}, t)$ and how can it be modeled? Recall that we are not talking about the *evolution* of the system from some state of “nothing”, but are focusing on the (dynamical) *steady-state* to which the system eventually evolves.

Two methods are useful for modeling such a steady-state of $q(\mathbf{x}, t)$.

For a strongly localized vortex—see, for example, Ref. [17]—quantity $q(\mathbf{x}, t)$ can be parameterized by a function in the form $F(\mathbf{x} - \mathbf{x}_0(t))$, i.e., the one with the center at coordinate $\mathbf{x} = \mathbf{x}_0(t)$, which satisfies the equation of transport $\dot{x}_{0k}(t) + \epsilon_{ik}\partial_i\psi = 0$. In other words, in such cases, the center of the vortex moves according to $\dot{\mathbf{x}}_0(t) - \mathbf{v}[\mathbf{x}_0(t)] = 0$. (Here, the symbol “dot” signifies the derivative with respect to time.)

Alternatively—as we will consider below—the distribution of $q(\mathbf{x}, t)$ can be described in the form of a macro-structure with “petals” (with constant $q(\mathbf{x}, t) = q_0$ inside) whose moving boundaries evolve according to Equation (6).

Extended (i.e., not narrowly localized) stationary vortex structures—the ones rotating with constant angular velocity $\omega (\equiv \omega_3)$ —are simpler to consider in a rotating coordinate system where the structures appear immovable, i.e., when their rotation direction is co-aligned with the z -axis and the derivative with respect to time becomes $\partial_t = -\omega\epsilon_{ik}x_i\partial_k$. (The procedure is laid out, for example, in Ref. [18].) Indeed, when $f = f(\rho, \phi - \omega t)$, then calculations relying on the properties of Jacobians produce the following: $\partial_t f = -\omega\partial_\phi f = -\omega\partial(f, \rho)/\partial(\phi, \rho) = -\omega(\partial(f, \rho)/\partial(x_1, x_2))(\partial(x_1, x_2)/\partial(\phi, \rho)) = -\omega(\epsilon_{ik}\rho^{-1}x_i\partial_k f)(-\rho)$. Then, Equation (5) may be rewritten as follows:

$$\epsilon_{ik}\partial_i \left(-\frac{\omega}{2}|\mathbf{x}|^2 + a\tau \right) \partial_k \left(\tau + \frac{\tau_1}{2}|\mathbf{x}|^2 \right) = 0, \tag{10}$$

which is satisfied by the ansatz

$$\tau + \frac{\tau_1}{2}|\mathbf{x}|^2 = F\left(-\frac{\omega}{2}|\mathbf{x}|^2 + a\tau\right). \tag{11}$$

The explicit expression of function F can be found from the obvious fact that temperature-driven flow perturbations must vanish when temperature perturbations vanish themselves. The suitable expression is as follows: function $F(u) = -\tau_1 u/\omega$. Then, temperature fluctuations are expressed as follows:

$$\tau = -\frac{\tau_1}{\omega}a\tau. \tag{12}$$

It follows from here that parameter $a = -\omega/\tau_1$. Combining this with Equation (4), where $\partial_t = -\omega\epsilon_{ik}x_i\partial_k$ is taken into account, we obtain the second evolution equation—the

one which describes the rotation of a stationary vortex structure with angular velocity ω caused by the self-induced field of hydrodynamical velocity:

$$\epsilon_{ik}(-\omega x_i + a\partial_i\tau)\partial_k(\Delta\tau - R^{-2}\tau) = 0. \tag{13}$$

Here, $R^2 = (\tau_1\beta)^{-1}(\omega/\Omega)^2 \equiv \lambda_\theta^2(\omega/\Omega)^2$, where the thermal length scale $\lambda_\theta = (\tau_1\beta)^{-1/2}$ characterizes the background regime of this model. Obviously, an extended (multi-petal) thermo-vortex structure exists when parameter τ_1 , characterizing the ‘‘rapidity’’ of the change in temperature (and stream function) with the distance from the disk rotation axis of $\tau_1 > 0$.

The ‘‘Blob’’ in The Method of Contour Dynamics / Sharp Boundaries Evolution Method (SBEM): The term ‘‘thermo-vortical blob’’ defines, in the plane (x_1, x_2) , a domain D filled with constant vorticity q_0 (with the dimensions $[q_0] = [time]^{-1}$) and bounded by a closed contour ∂D .

The contour can be described in the parametric form, where parameter s is the contour’s arc length (starting from some initial point on the contour), such that $0 < s < L$, where L is the entire length of the contour. The shape of the blob boundary is given by the following equations:

$$x(s) = v_1 \cos \phi - v_2 \sin \phi, \quad y(s) = v_1 \sin \phi + v_2 \cos \phi, \tag{14}$$

where the quantities v_1, v_2 , and ϕ are functions of s . Next, we introduce dimensionless variables and parameters: $\sigma = L/l, s \rightarrow Ls, \alpha = (\omega/q_0)(l/R)^3, \eta = \sigma/4K(m)$. Here, $K(m)$ is the complete elliptic integral of the first kind. Omitting the details of the analysis, we will only point out that the functions

$$v_1 = \frac{1}{8\alpha}\kappa', \quad v_2 = -1 + \frac{1}{16\alpha}\kappa_0^2 - \frac{1}{16\alpha}\kappa^2 \tag{15}$$

are linked with the curvature of the contour κ via the following non-linear differential equation:

$$\kappa'' + (8\alpha - \frac{1}{2}\kappa_0^2)\kappa + \frac{1}{2}\kappa^3 - 8\alpha = 0. \tag{16}$$

Here, prime signifies a derivative with respect to dimensionless argument σs . The angular coordinate $\phi(s)$ of the tracing point on the contour (Figure 2) is calculated from the following obvious expression:

$$\phi(s) - \phi(0) = \int_0^{\sigma s} d\xi \kappa(\xi) \tag{17}$$

which follows from the definition of curvature κ .

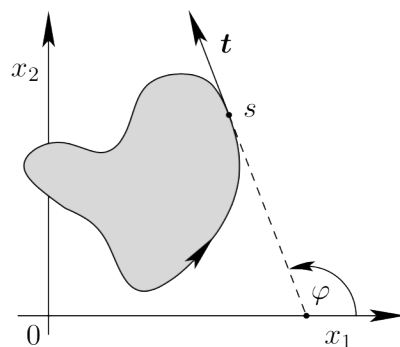


Figure 2. Illustration of a vortex blob.

Equation (16) resembles Duffing’s equation:

$$y'' + (1 - 2m)y + 2my^3 = 0, \tag{18}$$

which describes oscillations in a non-linear oscillator (see Ref. [19–22], for example). Equation (A34) is solved analytically in terms of Jacobi elliptic functions $y = cn(\theta, m)$ with period $4K(m)$. The non-zero free term 8α complicates the straightforward solving of Equation (16).

To bring the equation into a canonical form without the free term, we can make the following manipulations: make a “shift” in κ , “flip” the result “upside down”, make a change in the magnitude, make one more “shift” in the result, and finally, make a change in the magnitude again. In other words, the solution has the following form:

$$\kappa(s) = A + \frac{B}{1 - \epsilon z(\lambda s)} \tag{19}$$

where $z(\lambda s)$ is the Jacobi elliptic cosinus and $\lambda = n4K(m)$ for n -petal configuration: $n = 2, 3, \dots$. Parameter λ provides the periodicity of the solution ($z(0) = z(\lambda)$), i.e., the closing of the contour. Therefore, we change the argument, transitioning from σs to $\theta = \lambda s$. The initial conditions are introduced as $\kappa(0) = \kappa_0$ and $\kappa_{,s}(0) = 0$.

The solution contains six free parameters: $\alpha, \eta = \sigma/4K(m), A, B, m, \epsilon$. However, one parameter remains free; this fixes the values of all other parameters. We select ϵ as the controlling parameter. Parameter ϵ determines the magnitude of the initial perturbation because of $\kappa(0) = A + B/(1 - \epsilon)$. Obviously, for the unperturbed state, when $\epsilon = 0$, we have $A + B = 1, \sigma = 2\pi, m = 0, \phi(0) = \pi/2, \eta = 1$.

Omitting the details of calculations, we found

$$\begin{aligned} m &= \epsilon^2 \mu, \\ A &= \frac{(-1 + 2(-1 + \epsilon^2)\mu)(\epsilon^2 + \mu - 2\epsilon^3\mu - \epsilon^4\mu + 2\epsilon(1 + \mu))}{\epsilon^2 + \mu - \epsilon^4\mu}, \\ B &= \frac{2(1 - \epsilon^2)(1 + \mu - \epsilon^2\mu)(\epsilon^2 + \mu - 2\epsilon^3\mu - \epsilon^4\mu + 2\epsilon(1 + \mu))}{\epsilon^2 + \mu - \epsilon^4\mu}, \\ \alpha &= \frac{(\epsilon^2 + \mu - 2\epsilon^3\mu - \epsilon^4\mu + 2\epsilon(1 + \mu))^3}{8(\epsilon^2 + \mu - \epsilon^4\mu)^2}, \\ \eta &= -\frac{n(-\epsilon^2 - \mu + \epsilon^4\mu)}{(1 - \epsilon^2)^{1/2}(1 + \mu - \epsilon^2\mu)^{1/2}(\epsilon^2 + \mu - 2\epsilon^3\mu - \epsilon^4\mu + 2\epsilon(1 + \mu))}, \\ \sigma &= 4K(\epsilon^2\mu)\eta. \end{aligned} \tag{20}$$

Parameter $\mu(n, \epsilon)$ is fixed by the condition that the solution of equation

$$\frac{1}{\sigma}\phi_{,s} = \kappa(s) \rightarrow \frac{d\phi(s)}{ds} = 4K(\epsilon^2\mu)\eta \left(A + \frac{B}{1 - \epsilon cn(n4K(\epsilon^2\mu)s, \epsilon^2\mu)} \right) \tag{21}$$

has to satisfy the boundary conditions $\phi(0) = \pi/2$ and $\phi(1) = 5\pi/2$. Here, $cn(\xi, m)$ is the Jacobi elliptic cosinus, $K(m)$ is the complete elliptic integral of the first kind, $4K(0) = 2\pi$, and n is the number of petals in the vortex structure. In Equation (19), parameters A, B , and others, are taken from Equation (20); dimensionless parameter s changes from $s = 0$ to $s = 1$.

The calculation, which we do not present in this section, provides the leading term in the expansion of $\mu = \mu(n, \epsilon)$ in a series with respect to ϵ (which does not vanish when $\epsilon \rightarrow 0$): the expression $\mu \rightarrow n^2 - 1$.

3. Results

To analyze the thermo-vortical “blobs”, we employed the so-called Sharp Boundaries Evolution Method (SBEM). Within the blob, $q(\mathbf{x}, t) = q_0$ is constant; outside the blob, $q(\mathbf{x}, t) = 0$. This method originated in the 1960s–1970s and was further advanced in subsequent years. Despite the seemingly radical simplification, the method produces a reasonably good description and estimates for large-scale vortex flows/structures ([9,10]). Indeed, for the motion of an incompressible fluid in the xy -plane, the velocity vector \mathbf{v} lies in the same plane, and the vorticity vector has only one non-zero component, q_z . For large-scale vortex structures, it is intuitively apparent that there exist zones (which are sometimes rather spacious) where the vorticity magnitude reaches its maxima (“hilltops”) when the sign of vorticity is positive and its minima (“chasms”) when the sign of vorticity is negative. There are also zones where vorticity is zero or close to zero (“flats”), transitional zones between hilltops and flats (“upper slopes”), and transitional zones between flats and chasms (“lower slopes”). Since typically the fluid velocity and thermodynamical quantities are analyzed in terms of the integral characteristics derived from vorticity, when the slopes are steep (i.e., the Reynolds number Re or its equivalent is enormous), these transitional zones may be treated as sharp (precipitous, vertical) moving boundaries which evolve in accordance with the laws of hydrodynamic flows. In this paper—to not complicate the calculations—we consider only the case with the hilltops, upper slopes, and flats (not including the chasms and lower slopes).

One Coherent Multi-Petal Structure: We find that, because of the intertwined nature of the thermal and vortical fields in the fluid medium, what often looks like a group of *multiple individual “circular” vortices* (as depicted in Figure 1, for example) is in fact *one coherent macro-structure with a complex multi-petal shape*. In other words, the localized “circular” vortices are not independent; they influence each other, redistributing conservable quantities—such as vorticity $q(\mathbf{x}, t)$ and energy, which are linked to temperature $\tau(\mathbf{x}, t)$ —locally, within and between each other, while preserving the integrals over the entire multi-petal system.

Figure 3 illustrates the contours of thermo-vortices with three and five petals.

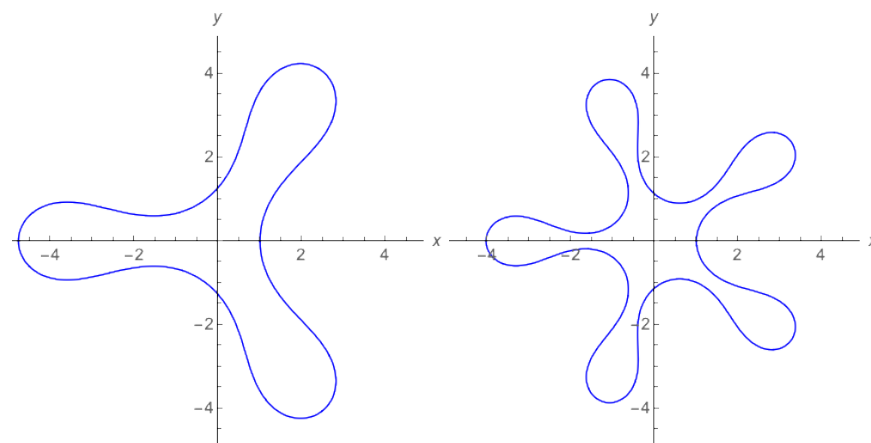


Figure 3. Examples of 3-petal and 5-petal contours.

Describing the shape of such a multi-petal structure mathematically is not a trivial exercise. We demonstrate how we characterize the shape using several key parameters: the number n of petals (counting the “fingers”), the level of non-linearity ϵ (describing whether the “fingers” are long or short; measuring the gap between the peak and trough); and parameter $\mu(n, \epsilon)$ (describing whether the “fingers” are thick or thin, and sharply pointed or not). The latter is achieved by employing (instead of “smooth” sinus/cosinus functions) the Jacobi elliptic sinus/cosinus, which permits the inclusion of higher spectral harmonics into the description of the shape’s “fullness”.

In Figure 3, both shapes have the same peak/trough nonlinearity, i.e., they possess the same parameter $\epsilon = -0.28$. But because they have a different number of petals n , their values of $\mu(n, \epsilon)$ are different. Figure 4 illustrates how $\mu(n = 3, \epsilon)$ depends on ϵ and how parameter ϵ (and therefore $\mu(n, \epsilon)$) impacts the contour shape.

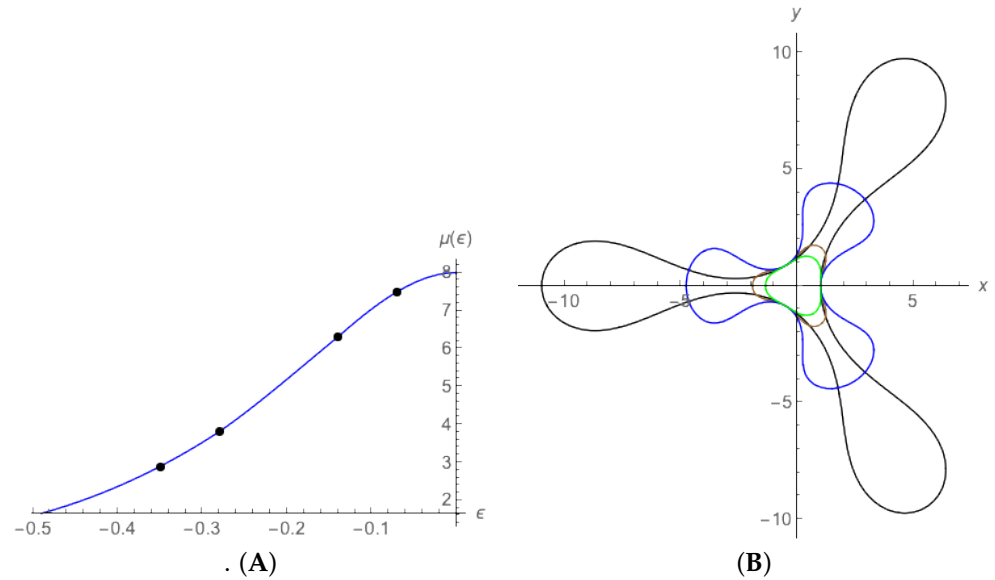


Figure 4. Impact of nonlinearity (peak/trough) parameter ϵ on a three-petal thermo-vortex. **Left panel (A):** Plot for $\mu(n = 3, \epsilon)$. Dots correspond to examples in Panel 3B. Maximum μ is at $\epsilon = 0$: $\mu_{max}(n, 0) = n^2 - 1$. **Right panel (B):** Deformation of three-petal contour: $\epsilon = -0.07$ (green; inner); $\epsilon = -0.14$ (brown); $\epsilon = -0.28$ (blue); $\epsilon = -0.35$ (black; outer).

Parameter $\mu = \mu(n, \epsilon)$ is not an independent quantity. It can be found via the imposition of one more condition: the requirement that the contour must close, i.e., that phase difference $\phi(1) - \phi(0) = 2\pi$, which follows from Equation (21). For moderate $-0.49 \leq \epsilon \leq 0$ and $2 \leq n \leq 8$, function $\mu(n, \epsilon)$ is well approximated by the simple expression $\mu(n, \epsilon) \simeq (n^2 - 1) / (1 + c\epsilon^2(n^2 - 1))^d$, where $c \simeq 1.56$ and $d \simeq 0.98$.

Figure 5 illustrates how $\mu(n, \epsilon)$ behaves for varying numbers of petals n and nonlinearity (peak/trough) parameter ϵ .

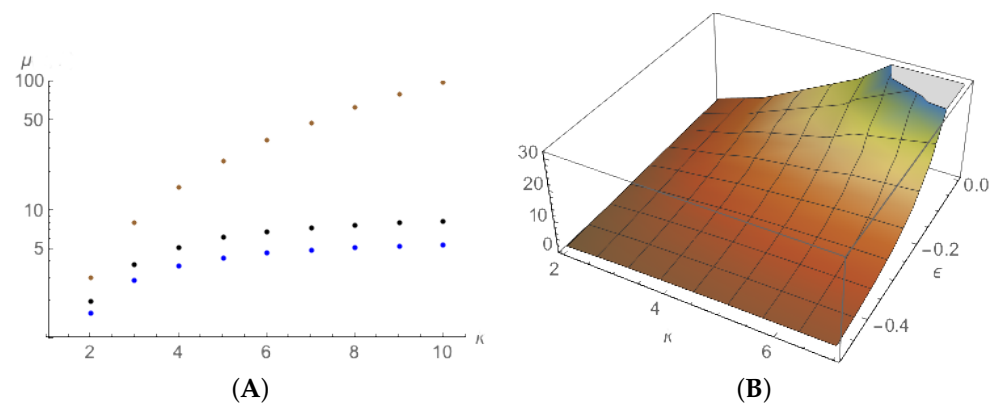


Figure 5. Sensitivity of $\mu(n, \epsilon)$ to the number of petals n and nonlinearity (peak/trough) parameter ϵ . **Left panel (A):** Vertical μ -axis is logarithmic. Curves denote the following: $\epsilon = -10^{-3}$ (brown; upper); $\epsilon = -0.28$ (black); $\epsilon = -0.35$ (blue; lower). **Right panel (B):** Vertical μ -axis is linear and cut off at $\mu = 30$ for better clarity of the image.

Once the shape of the contour of the macro-structure can be described, the properties of the system can be analyzed.

Number of Petals and Other Key Parameters: Generally speaking, the number of petals n evolves as the system evolves because of the complex linkage between the parameters in the system. Physically, multi-petal vortex structures arise when thermal energy is introduced into the system, leading to the formation of a hot ($\tau_0 \neq 0$) domain of finite ($0 < l < \infty$) size with non-zero vorticity ($Q \neq 0$) inside. Mathematically, when three quantities Q , l , and τ_0 are specified as the initial conditions, they “fix” three geometrical parameters: n , ϵ , and μ . Here, the conserved quantity is as follows:

$$Q = q_0 l^2 \sigma \frac{1}{2} I_n(\epsilon, \mu), \text{ where } I(\epsilon, n) = \int_0^1 ds \left((v_1^2(s) + v_2^2(s)) \kappa(s) \right). \quad (22)$$

Recall that here, l is the characteristic size; $\sigma \equiv L/l$, where L is the contour length; parameter s is the contour’s arc length.

Quantities l and τ_0 may be measured in observations. Thus, their links to other parameters in the system are informative:

$$l = \left(\frac{2}{I_n}\right)^{1/5} \alpha^{1/5} \sigma^{-1/5} \left(\frac{QR^3}{\omega}\right)^{1/5}, \quad \tau_0 = \left(\frac{2}{I_n}\right)^{3/5} \alpha^{-2/5} \sigma^{-3/5} \tau_1 \left(\frac{QR^{4/3}}{\omega}\right)^{3/5}. \quad (23)$$

All coefficients are functions of ϵ , n , and μ . The dimensions of the quantities $[Q] = \text{length}^2 \times \text{time}^{-1}$, $[R] = \text{length}$, $[\omega] = \text{time}^{-1}$ and $[\tau_1] = \text{temperature} \times \text{length}^{-2}$ assure the correct dimensions of the written expressions for l and τ_0 .

Temperature Distribution: Determination of the contour is the first step of the analysis. Once the steady-state contour for the thermo-vortical blob is established, the temperature distribution $\tau = \tau(t, x_j)$ inside the blob may be determined. The expression for temperature distribution in terms of dimensionless variables is as follows:

$$\tau(x, y) = \left(\frac{q_0 \tau_1 R^2}{2\pi\omega}\right) (\beta\sigma) \int_0^1 ds \left(\frac{1}{\beta|\hat{z} - z|} - \frac{1}{2} K_1(\beta|\hat{z} - z|) \right) \Re \left(\frac{\exp[i\phi(s)](\hat{z}^* - z^*)}{i|\hat{z} - z|} \right). \quad (24)$$

Figure 6 shows—for the same study—the vorticity distribution $q(x, y)$ and the temperature profile (in the xz -plane for $y = 0$; obviously, temperature is distributed similarly within the planes slicing the other petals). The right panel also shows how the temperature profile varies depending on the geometrical parameter $\beta = l/R$. The greater β is, the “tighter” the thermal structure within the petal—the petal peak is higher, the sides are narrower, and also, near the center of macro-rotation, the central thermo-vortex appears.

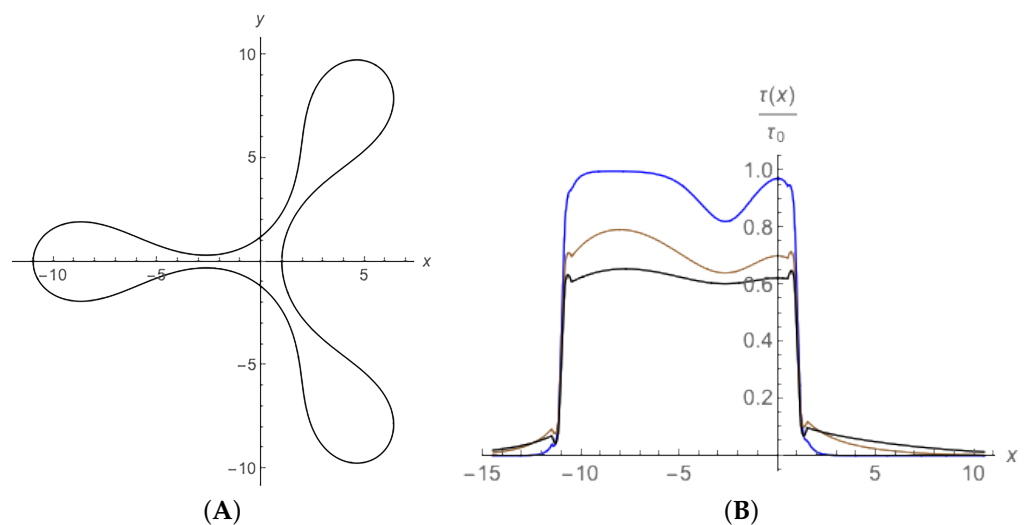


Figure 6. Left panel (A): Vorticity distribution $q(x)$ of the three-petal thermo-vortical structure. Right Panel (B): Temperature distribution when $y = 0$ and geometrical parameter $\beta = l/R$ is as follows: $\beta = 1/\pi$ (black; lower curve), $\beta = 2/\pi$ (brown), and $\beta = \pi$ (blue; upper curve).

4. Discussion and Conclusions

The fact that rotating cosmic fluids contain vortices has been understood for a while. Vortices have been discussed in the context of planetary atmospheres (at least since the discovery of the Jupiter's Great Red Spot), in the context of vortices and magnetic flux tubes in the accretion disks of black holes [23], galactic center hot spots [24], and so on. When the observed vortices are multiple, coherent, and long-lasting, they are also often clustered into orderly quasi-symmetric arrangements. These multiple vortices are typically interpreted as possibly interacting, but nonetheless as *stand-alone* items.

In our paper, we demonstrated that an additional physical interpretation of what these vortices represent may exist. What one sees in astronomical images as distinct spots may be not *multiple individual quasi-circular-shaped vortices*, which possibly interact and drift to form a quasi-symmetrical quasi-stationary macro-arrangement, but instead these distinct spots (thermo-vortices) may be the observable parts of *one structure* whose shape is a complex contour with multiple "petals". Either alternative is theoretically possible, but the latter one is typically not considered.

To bring attention to this multi-petal interpretation, we presented and analyzed a model that can be illustrative and adaptable to various environments. Specifically, in order for our model to be of interest for studies of the accretion disks of black holes, we used the metric that works for the mildly curved spacetime (naturally, this model works in flat spacetime as is the case for planets). We had to limit our considerations to the model of a rotating "thin" layer because otherwise the mathematical calculations would become unwieldy. Our focus was on the description of the *steady-state*, large-scale, thermo-vortical motions, not on the evolution from the state of "nothing". We demonstrated that the steady-state may indeed look like a multi-petal structure and that the shape of individual petals may be highly nonlinear (the petals may look like "fat fingers", or be elongated or pointy). Various parameters (relative dimensions of the system, thermal gradient, initial vorticity, etc.) and their linkages determine the outcome. We also demonstrated that the petals indeed have an elevated temperature and would appear as bright spots if observed from afar.

The physical explanation for why a system would evolve towards a steady-state with N petals rather than M petals is intuitively simple. The contour of the macro-structure bounds the inner domain of higher vorticity. Naturally, the contour is closed. Therefore, if subjected to some perturbation, the contour's steady-state turns into a "standing wave" (like a standing wave on the surface of a swimming pool), with the number of crests (petals) defined by the properties of the system. The shape of the crests, however, is not sinus-wave-like but is complex (finger-like) because the system is highly nonlinear. Obviously, no steady-state is eternal, but we did not study the problem of the transition of quasi-steady-states.

Several notable multi-vortex arrangements, which are likely to be multi-petal structures, can be mentioned. As seen in Figure 1 (second row; panels C and D), in the span of one year, the Antarctic ozone hole evolved from a quasi-circular into a two-petal structure. Based on the common knowledge of what the ozone hole represented, we can conclude with certainty that the two vortices observed in 2002 were not separate entities; they were indeed two petals of one shape-changing macro-structure. The arrangement of vortices on Jupiter's South Pole (Figure 1B) is also a candidate multi-petal macro-structure. Specialists in geophysical fluid dynamics may spot an analogy between the study of this paper and the Rossby waves (see, e.g., Ref. [25]): the interface on the thermocline η (or, equivalently, the streamfunction) corresponds to the temperature τ (which is proportional to the streamfunction due to the presumed Equation (2)), the pressure gradient responsible for the geostrophic flow corresponds to the gradient of the centrifugal potential Φ , and the potential vorticity corresponds to the q -vorticity. Not surprisingly, the global nature of planetary solitary waves corresponds to multi-petal structures and explains images like those in Figure 1B–D. One difference, however, is that the Rossby waves occur at the sharp

boundaries between regions with different temperatures; in our case, the regions are of different vorticities.

As for the question of whether our mathematical treatment is valid for a “thick” system—such as the atmosphere of Jupiter or a “thick” double-layered accretion disk near a rotating black hole—the answer is yes. “Thick” systems may be, in principle, described using the same mathematical apparatus when the vorticity patch is broken into columnar sub-patches. (Refs. [9,10] point to the use of this technique.)

For a more detailed treatment—not included in this paper—it is necessary to consider the nuances of mathematical models for hydrodynamic flows (see, for example, Refs. [26,27]), collective plasma effects [28], relativism [29–43], and relativistic hydrodynamics [44].

For a strongly relativistic system—such as an accretion disk in the environment of a rapidly rotating supermassive object or a supermassive black hole, see Refs. [45–47]—the conditions (in covariant description) of adiabaticity and incompressibility remain the same, while the equation of fluid motion (in spacetime with a metric defined by the square of the four-interval $ds^2 = m_{ik}dq^i dq^k$ in the equatorial plane of a rotating black hole when the coordinate $q^2 \equiv \theta = \pi/2$) has the following form in the leading approximation (these details of our analysis are not listed in this paper):

$$-\frac{w}{c^2} Dv_\beta = \partial_\beta p + 2\frac{w}{c^2} [\mathbf{v} \times \boldsymbol{\Omega}]_\beta + w\partial_\beta \ln \sqrt{g_{00}} + \dots \quad (25)$$

Here, D is the operator of the total derivative with respect to the “synchronized time”; the enthalpy w is defined as $w/c^2 = \gamma\rho + (1/c^2)(\rho e_1 + p)$, where γ is the Lorentz factor, p is the pressure, and e_1 is the non-relativistic part of the internal energy; c is the light speed; v_β is the covariant β -component of the 3D velocity. Naturally, the basic elements of the model momentum in Equation (A84) are the pressure gradient (the first term), the “Coriolis force” (the second term), and the gravity and centrifugal forces, which are packed in the third term of the momentum equation. The key difference compared to the classic hydrodynamic treatment is the replacement of the classic gravity/centrifugal acceleration $-\nabla\Phi + \Omega^2\mathbf{r}$ with $-\nabla \ln \sqrt{m_{00}}$, and the replacement of the classic averaged angular velocity Ω of the accretion disk rotation with the relativistic parameter $\boldsymbol{\Omega} = (c/2)\gamma u^0 \text{curl}(-g_{00}\mathbf{g})$. If the thermo-vortices are at some “distance” from the event horizon and conditions $x = r/r_g \gg 1$, $\Omega x < 1$ are satisfied, then, leaving the leading terms in the expansion $\partial_\beta \ln \sqrt{m_{00}}$, we can obtain that $\partial_\beta \ln \sqrt{m_{00}} \simeq -x\Omega^2 + 1/2x^2 + 1/2x^3 + (2a + \Omega)\Omega/2x^2$. Here, the terms of higher orders of smallness are omitted. The first term describes the centrifugal effect, the second describes the contribution of the force of attraction in the Newtonian approximation of gravity, the third term describes the Schwarzschild model of a non-rotating black hole, the last takes into account the rotation of both the black hole and the disk. For $x \gg 1$, $\Omega x < 1$, but $\Omega x^{3/2} > 1/2$, the principal contribution provides the first term $\sim \Omega^2$, i.e., the centrifugal effect, independent of the exact structure of the spacetime near the rotating, or not rotating, black hole.

To conclude, the illustrative model that we presented provides insights that are useful for a broad range of physical applications, ranging from planetary atmospheres to black hole accretion disks. Whether the observed vortices in cosmic fluids are conceptualized as stand-alone objects or inextricable parts of one macro-structure may meaningfully influence the numerical models employed in consideration of the phenomena and image reconstruction methods.

Author Contributions: Conceptualization and writing, E.P.T. and V.I.P. All authors have read and agreed to the published version of the manuscript.

Funding: This research received no external funding.

Data Availability Statement: No new data were created or analyzed in this study. Data sharing is not applicable to this article.

Conflicts of Interest: The authors declare that there is no conflict of interests regarding the publication of this article.

Appendix A. The Concept of “Thermo-Vorticial Blob”

The material in Appendix A is presented for the readers unable to read (in its original, and only, language of publication) one the foundational sources—the book (Ref. [9]) by V.P. Goncharov and one of the authors of this article—which, among many things, examines the core considerations regarding the use of a complex variable functions set, required for the implementation of the method here called the Sharp Boundaries Evolution Method (SBEM), in detail. The method—laid out and applied in examples in Refs. [9,10,18]—relies on the concept of “a thermo-vorticial blob”.

The term “a vorticial blob” is defined (in the complex plane $z = x_1 + ix_2$) as a region (domain D) filled with constant vorticity (q_0 , with dimensions $[q_0] = [time]^{-1}$) and bounded by a closed contour (∂D). When convenient, we will use coordinate notations $\mathbf{x} = (x_1, x_2)$, as well as $\mathbf{x} = (x, y)$. See Figure 2.

The contour can be described in the parametric form $\hat{z} = \hat{z}(s)$, where parameter s is the contour’s arc length (starting from some initial point on the contour) such that $0 < s < L$, where L is the entire length of the contour. The derivative $\hat{z}_{,s} \equiv \partial\hat{z}/\partial s$ is obviously the unit-vector tangential to the contour. The normalizing condition follows from the definition of the tangential unit vector:

$$|\hat{z}_{,s}(s)|^2 = 1, \tag{A1}$$

which can be also expressed as follows:

$$\hat{z}_{,s}(s) = \exp(i\phi(s)). \tag{A2}$$

The contour is traced in the counterclockwise direction. The tangential unit vector $\hat{z}_{,s}$ is colinear to the x_2 -axis when $s = 0$. Consequently, $\phi(0) = \pi/2$.

Therefore, the contour can be described as follows:

$$\hat{z}(s) = \exp(i\phi(s))(v_1(s) + iv_2(s)), \tag{A3}$$

where $v_1(s)$ and $v_2(s)$ must satisfy the following conditions:

$$v_{1,s}(s) - \kappa(s)v_2(s) = 1, \quad v_{2,s}(s) + \kappa(s)v_1(s) = 0, \quad \phi_{,s}(s) - \kappa(s) = 0 \tag{A4}$$

for any values of parameter s (here, $\kappa(s)$ is the curvature of the contour at the tracing point s). Indeed, if, at $s = 0$, the radius vector is colinear with the x -axis (hence, the angle is $\pi/2$ for the tangent vector), then $v_1(0) = 0$ and $v_2(0) = -l$. The components of these two vectors are equal to $\hat{z}(0) = (l, 0)$ and $\hat{z}_{,s}(0) = (0, i)$, respectively.

The equations describing the contour profile are thus:

$$\hat{x} = \hat{v}_1 \cos \phi - \hat{v}_2 \sin \phi, \quad \hat{y} = \hat{v}_1 \sin \phi + \hat{v}_2 \cos \phi, \quad \phi_{,s} = \kappa. \tag{A5}$$

To describe the vortex blob analytically, we will use the two-dimensional Heaviside function $\Theta(z)$, defined as follows:

$$\begin{aligned} \Theta(z) &= 1, \text{ if } z \in D, \text{ and } \Theta(z) = 0, \text{ if } z \notin D, \\ \Theta(z) &= 1/2, \text{ if } z \text{ is on contour } \partial D. \end{aligned} \tag{A6}$$

The vorticity distribution ($q \sim \text{curl}v$) for a vortex blob may then be written as follows: $q = q_0\Theta(z)$.

In the complex plane, the $\Theta(z)$ -function can be written in the form of the contour integral (see Refs. [19,26], for details), where the contour is traced in the counterclockwise direction:

$$\Theta(z) = \frac{i}{2\pi} \int_{\partial D} \frac{d\hat{z}}{z - \hat{z}}. \tag{A7}$$

Equation (A7) is, obviously, a corollary of the Cauchy theorem. Equation (A7) can be rewritten in the following form:

$$\Theta(z) = \frac{i}{2\pi} \int_0^L ds \frac{\hat{z}_{,s}(s)}{z - \hat{z}(s)} = -\frac{i}{2\pi} \int_0^L ds \frac{\hat{z}_{,s}(s)}{|\hat{z}(s) - z|} \frac{\hat{z}^*(s) - z^*}{|\hat{z}(s) - z|}. \tag{A8}$$

With the help of two useful formulae (see Ref. [19])

$$\frac{\partial}{\partial z^*} \left(\frac{1}{z} \right) = \pi \delta^{(2)}(x_1, x_2) \quad \text{and} \quad \frac{\partial}{\partial z} \left(\frac{1}{z^*} \right) = \pi \delta^{(2)}(x_1, x_2), \tag{A9}$$

the derivatives of Θ -function with respect to z^* and z may be expressed in form of the contour integral:

$$\begin{aligned} \frac{\partial \Theta(z)}{\partial z^*} &= \frac{i}{2} \int_{\partial D} ds \hat{z}_{,s}(s) \delta^{(2)}(\mathbf{x} - \hat{\mathbf{x}}(s)), \\ \frac{\partial \Theta(z)}{\partial z} &= -\frac{i}{2} \int_{\partial D} ds \hat{z}_{,s}^*(s) \delta^{(2)}(\mathbf{x} - \hat{\mathbf{x}}(s)). \end{aligned} \tag{A10}$$

Appendix A.1. Temperature Distribution

The introduction of the so-called ψ -function, defined as $\psi \equiv a\tau$, helps simplify derivations. Indeed, vorticity $q \sim q_0 \sim \text{curl} \mathbf{v}$ is a local characteristic, which determines the magnitude of the vortex motion in the structure, whereas temperature τ depends on the characteristics of the environment (ω, τ_1, \dots). The ψ -function is a local solution of the corresponding Green equation

$$\psi(\mathbf{x}) = -\frac{1}{2\pi} \int d\mathbf{x}' q(\mathbf{x}') K_0\left(\frac{|\mathbf{x} - \mathbf{x}'|}{R}\right) = -\frac{q_0}{2\pi} \int d\mathbf{x}' \Theta(\mathbf{x}') K_0\left(\frac{|\mathbf{x} - \mathbf{x}'|}{R}\right). \tag{A11}$$

Here, $d\mathbf{x} = dx_1 dx_2$ is a surface element of the xy -plane; function $K_0(\xi)$ denotes a modified Bessel function of the 0-th order. Since $K_0(\xi)$ is the Green function (see, for example, Ref. [48]),

$$\left(\Delta - \frac{1}{R^2} \right) \left(-\frac{1}{2\pi} K_0\left(\frac{|\mathbf{x} - \mathbf{x}'|}{R}\right) \right) = \delta^{(2)}(\mathbf{x} - \mathbf{x}'), \tag{A12}$$

we can rewrite Equation (A11) as follows:

$$\begin{aligned} \psi(\mathbf{x}) &= -\frac{q_0}{2\pi} \int d\mathbf{x}' \Theta(\mathbf{x}') \left(2\pi R^2 \delta^{(2)}(\mathbf{x}' - \mathbf{x}) + R^2 \Delta' K_0\left(\frac{|\mathbf{x}' - \mathbf{x}|}{R}\right) \right) = \\ &= -\frac{q_0}{2\pi} \int d\mathbf{x}_1 \Theta(\mathbf{x}_1) \left(2\pi R^2 \delta^{(2)}(\mathbf{x}_1 - \mathbf{x}) + R^2 \frac{\partial^2}{\partial z_1^* \partial z_1} K_0\left(\frac{|z_1 - z|}{R}\right) \right). \end{aligned} \tag{A13}$$

The Laplace operator (with respect to the running coordinates with index 1) is obviously $\Delta_1 \equiv \partial_1^2 + \partial_2^2 = (\partial_1 + i\partial_2)(\partial_1 - i\partial_2) = \partial^2 / \partial z_1^* \partial z_1$. From here, we can obtain the following:

$$\psi(\mathbf{x}) = -q_0 R^2 \Theta(\mathbf{x}) - \frac{q_0 R^2}{2\pi} \int d\mathbf{x}_1 \Theta(z_1) \frac{\partial^2}{\partial z_1^* \partial z_1} K_0\left(\frac{|z_1 - z|}{R}\right). \tag{A14}$$

Integrating (with respect to z_1^*) Equation (A14) by parts and using known transformations for the Bessel functions, we find that

$$\psi(\mathbf{x}) = -q_0R^2\Theta(\mathbf{x}) - \frac{q_0R}{4\pi} \int d\mathbf{x}_1 K_1\left(\frac{|z_1 - z|}{R}\right) \times \left(\frac{\partial\Theta(z_1)}{\partial z_1^*}\right) \frac{(z_1^* - z^*)}{|z_1 - z|} + \left(\frac{\partial\Theta(z_1)}{\partial z_1}\right) \frac{(z_1 - z)}{|z_1 - z|}. \tag{A15}$$

Next, we use Equation (A10) and change the integrating order. We find the following:

$$\psi(\mathbf{x}) = -q_0R^2\Theta(\mathbf{x}) - \frac{q_0R}{4\pi} \int_0^L du K_1\left(\frac{|\hat{z}(u) - z|}{R}\right) \frac{1}{2|\hat{z}(u) - z|} \times i\left(\hat{z}_{,u}(u)(\hat{z}(u)^* - z^*) - \hat{z}_{,u}^*(u)(\hat{z}(u) - z)\right). \tag{A16}$$

Since functions ψ and τ are connected by Equation (12), via $\tau = -(\tau_1/\omega)\psi$, we obtain, for the temperature distribution:

$$\tau(\mathbf{x}) = \frac{\tau_1q_0R^2}{\omega}\Theta(\mathbf{x}) - \frac{\tau_1q_0R}{4\pi\omega} \int_0^L ds K_1\left(\frac{|\hat{z}(s) - z|}{R}\right) \times \Im\left(\exp[i\phi(s)] \frac{(\hat{z}(s)^* - z^*)}{|\hat{z}(s) - z|}\right). \tag{A17}$$

Transitioning to dimensionless variables ($s \rightarrow Ls$, $z \rightarrow lz$, $\hat{z} \rightarrow l\hat{z}$, $l/R \rightarrow \beta$, $L/l \rightarrow \sigma$)—note that we preserve the same symbols for efficiency—we can rewrite Equation (A17) in the following form:

$$\tau(\mathbf{x}) = \tau_0(\Theta(\mathbf{x}) + G(\mathbf{x}; \beta)), \tag{A18}$$

where

$$G(\mathbf{x}; \beta, \sigma) = -\frac{\beta\sigma}{4\pi} \int_0^1 d\zeta K_1(\beta|\hat{z}(\zeta) - z|) \times \Im\left(\exp[i\phi(\zeta)] \frac{(\hat{z}(\zeta)^* - z^*)}{|\hat{z}(\zeta) - z|}\right). \tag{A19}$$

Parameter $\tau_0 = \tau_1q_0R^2/\omega$ is the parameter which determines the characteristic temperature level of the vortical blob. The integral Equation (A19) is a function of coordinates $\mathbf{x} = (x, y)$ which depend on the dimensionless geometrical parameters $\beta = l/R$ (the ratio of the blob size l to the “thermal” scale R) and $\sigma = L/l$ (the ratio of the contour length L to the characteristic blob size l). Recall that τ_1 , with dimension $[\tau_1] = [temperature]/[length]^2$, is the parameter characterizing the “rapidity” of the increase in basal temperature τ_s with distance from the rotation axis.

Appendix A.2. Value of ψ -Function for Blob Contour

To find the expression for the contour, we first transition from $\mathbf{x} \rightarrow \hat{\mathbf{x}}(s)$. Then, from Equation (A16), we obtain the following for $\hat{\psi} = \psi(\hat{z}(s))$:

$$\hat{\psi} = -q_0R^2\Theta(\hat{z}(s)) + \frac{q_0R}{4\pi} \int_0^L du K_1(R^{-1}|\hat{z}(u) - \hat{z}(s)|) \times \Im\left(\frac{\hat{z}_{,u}(u)(\hat{z}(u)^* - \hat{z}(s)^*)}{|\hat{z}(u) - \hat{z}(s)|}\right), \tag{A20}$$

where the variables are still dimensional.

We assume that parameter R is small in comparison with the characteristic scale of the blob. Then, the main contribution to the integral comes from a small region in the neighborhood of the tracing point $\hat{z}(s)$. The contour may possess some (small) curvature (meaning $|\hat{z}_{,ss}| \ll R^{-1}$). In the vicinity of point s (with small $\nu = u - s$ and $\hat{z}_{,ss} = i\hat{\kappa}\hat{z}_{,s}$ where $\hat{\kappa}(s) = \phi_{,s}$) we can write the following:

$$\begin{aligned} & \hat{z}_{,u}(u)(\hat{z}(u)^* - \hat{z}(s)^*) = \\ (\hat{z}_{,s} + \hat{z}_{,ss}\nu + \dots)(\hat{z}_{,s}^*\nu + \frac{1}{2}\hat{z}_{,ss}^*\nu^2 + \dots) &= \hat{z}_{,s}\hat{z}_{,s}^*\nu + \frac{1}{2}\hat{z}_{,s}\hat{z}_{,ss}^*\nu^2 + \hat{z}_{,ss}\hat{z}_{,s}^*\nu^2 + \dots = \\ |\hat{z}_{,s}|^2(\nu - i\frac{1}{2}\hat{\kappa}\nu^2 + i\hat{\kappa}\nu^2 + \dots) &= \nu + \frac{i}{2}\hat{\kappa}\nu^2 + \dots \end{aligned} \tag{A21}$$

Here, all terms of order $\geq \nu^3$ are omitted.

Equation (A20) is written (for a small curvature of ∂D) as a sum of two integrals: the first one, due to symmetrical limits, yields zero; the second—not zero:

$$\hat{\psi} = -\frac{1}{2}q_0R^2 + \frac{q_0R}{8\pi}\hat{\kappa}(s) \int_{-\infty}^{\infty} d\nu K_1\left(\frac{|\nu|}{R}\right) \frac{\nu^2}{|\nu|}. \tag{A22}$$

Here, both limits of integration ($\pm\infty$) stretch to infinity (keep in mind the exponential nature of the decrease in the Bessel function with the increasing value of its argument). The value of the integral is πR^2 . Accordingly, we obtain the final result:

$$\hat{\psi} = -\frac{1}{2}q_0R^2 + \frac{q_0R^3}{8}\hat{\kappa}(s). \tag{A23}$$

This expression establishes the link between the values of $\hat{\psi}$ -function (temperature) on the contour and its local curvature $\hat{\kappa}$.

Appendix A.3. Core Equations for Multi-Petal Structures

The boundary condition for the stream-function ψ on the contour, due to the presence of the Heavyside function in q and, therefore, the delta-function in its derivative, is

$$\hat{\psi} - \frac{\omega}{2}|\hat{\mathbf{x}}|^2 = Const. \tag{A24}$$

Using Equation (A23), Equation (A24) can be rewritten in the following form:

$$\frac{q_0R^3}{8}\hat{\kappa} - \frac{\omega}{2}|\hat{z}(s)|^2 = K_1, \tag{A25}$$

where $\hat{z}(s) = \hat{x}(s) + i\hat{y}(s)$. The constant of integration K_1 is fixed by the initial conditions $\hat{\kappa}_0, \hat{v}_1(0) = 0$ and $\hat{v}_2(0) = -l$; hence

$$K_1 = \frac{q_0R^3}{8}\hat{\kappa}_0 - \frac{\omega}{2}l^2. \tag{A26}$$

Then,

$$\hat{\kappa} = \hat{\kappa}_0 - 4\left(\frac{\omega}{q_0}\right)\frac{l^2}{R^3} + 4\left(\frac{\omega}{q_0}\right)\frac{1}{R^3}(\hat{v}_1^2 + \hat{v}_2^2). \tag{A27}$$

By taking the derivatives, we obtain the following:

$$\begin{aligned} \hat{v}_{1,s} - \hat{\kappa}\hat{v}_2 &= 1, \quad \hat{v}_{2,s} + \hat{\kappa}\hat{v}_1 = 0 \quad \text{and} \\ \hat{\kappa}_{,s} &= 8\left(\frac{\omega}{q_0}\right)\frac{1}{R^3}(\hat{v}_1\hat{v}_{1,s} + \hat{v}_2\hat{v}_{2,s}). \end{aligned} \tag{A28}$$

Using the first two equations, Equation (A28) can be written as follows:

$$\begin{aligned} \hat{v}_{1,s} - \hat{\kappa}\hat{v}_2 &= 1, & \hat{v}_{2,s} + \hat{\kappa}\hat{v}_1 &= 0, & \hat{\phi}_s - \hat{\kappa} &= 0 & \text{ and} \\ \hat{\kappa}_s - 8\left(\frac{\omega}{q_0}\right)\frac{1}{R^3}\hat{v}_1 &= 0. \end{aligned} \tag{A29}$$

with initial conditions $\hat{v}_1(0) = 0, \hat{v}_2(0) = -l, \phi(0) = \pi/2, \hat{\kappa}(0) = \hat{\kappa}_0$.

After solving Equation (A29), the expression for contour ∂D can be found using the following:

$$\hat{x} = \hat{v}_1 \cos \phi - \hat{v}_2 \sin \phi, \quad \hat{y} = \hat{v}_1 \sin \phi + \hat{v}_2 \cos \phi. \tag{A30}$$

We now introduce dimensionless variables and parameters: $\hat{v}_1 \rightarrow lv_1, \hat{v}_2 \rightarrow lv_2, \hat{\kappa} \rightarrow l^{-1}\kappa, \sigma = L/l, s \rightarrow Ls, \alpha = (\omega/q_0)(l/R)^3$. Equation (A29) becomes

$$v'_1 - \kappa v_2 = 1, \quad v'_2 + \kappa v_1 = 0, \quad \phi' - \kappa = 0, \quad \kappa' - 8\alpha v_1 = 0 \tag{A31}$$

with the initial conditions $v_1(0) = 0, v_2(0) = -1, \kappa(0) = \kappa_0$ and $\phi(0) = \pi/2$. Symbol “prime” signifies the derivative with respect to dimensionless argument $\xi = \sigma s$.

The unperturbed state of Equation (A31) is the one satisfied by $\kappa(s) = 1, v_1(s) = 0, v_2(s) = -1, \sigma = 2\pi$.

It may appear that one can simply solve the system in Equation (A31) numerically. Indeed, the solutions depend on one variable s and are fixed by two dimensionless parameters: parameter $\alpha = (\omega/q_0)(l/R)^3$ and phase parameter σ . The local curvature of contour κ_0 at the initial point is the governing parameter. Since we are dealing with differential equations with first-order derivatives and are given initial conditions, obtaining a numerical solution is not difficult. However, we are only interested in the solution that will “close” the contour, i.e., the tracing point must return to the starting point. This means that one more requirement must be added to the system.

Appendix B. Equations Permitting Analytical Solution

Aiming to find the equation for the blob contour, we first rewrite Equation (A31) in the following form:

$$\begin{aligned} v_1 &= \frac{1}{8\alpha}\kappa', & v_2 &= -1 + \frac{1}{16\alpha}\kappa_0^2 - \frac{1}{16\alpha}\kappa^2, \\ \frac{1}{8\alpha}\kappa'' - \kappa\left(-1 + \frac{1}{16\alpha}\kappa_0^2 - \frac{1}{16\alpha}\kappa^2\right) - 1 &= 0, \end{aligned} \tag{A32}$$

which may be further rewritten as follows:

$$\kappa'' + \left(8\alpha - \frac{1}{2}\kappa_0^2\right)\kappa + \frac{1}{2}\kappa^3 - 8\alpha = 0. \tag{A33}$$

Equation (A33) resembles the non-linear Duffing’s equation:

$$y'' + (1 - 2m)y + 2my^3 = 0, \tag{A34}$$

which is known (see Ref. [20–22], for example) to be solved analytically in terms of Jacobi elliptic functions $y = cn(\theta, m)$ with the period $4K(m)$. Here, $K(m)$ is the complete elliptic integral of the first kind. The non-zero free term 8α complicates the straightforward solving of Equation (A33).

The angular coordinate $\phi(s)$ of the tracing point on the contour is calculated from the obvious expression

$$\phi(s) - \phi(0) = \int_0^{\sigma s} d\eta \kappa(\eta) \tag{A35}$$

which follows from the definition of curvature κ .

Equation (A33) can be rewritten in the form of an equation of the first order with the constant of integration fixed by the initial condition imposed on $\kappa'(0)$:

$$(\kappa')^2 + (8\alpha - \frac{1}{2}\kappa_0^2)\kappa^2 + \frac{1}{4}\kappa^4 - 16\alpha\kappa = C_2, \tag{A36}$$

with the initial condition $\kappa(0) = \kappa_0$. When $\kappa'(0) = 0$, Equation (A33) becomes

$$\begin{aligned} (\kappa')^2 + (16\alpha\kappa_0 - \frac{1}{4}\kappa_0^4 - 8\alpha\kappa_0^2 + \frac{1}{2}\kappa_0^4) + \\ (-16\alpha)\kappa + (8\alpha - \frac{1}{2}\kappa_0^2)\kappa^2 + \frac{1}{4}\kappa^4 = 0. \end{aligned} \tag{A37}$$

Appendix B.1. Weakly Perturbed Contour: Linear Approximation

Equation (A33) is satisfied by $\kappa_0 = 1, \kappa(\theta) = 1$. This case corresponds to a circle (a contour with a constant curvature).

Now consider a small initial perturbation of the contour $\kappa(0) = k_0 \rightarrow 1 + \epsilon$. We can further write $\kappa(\theta) = 1 + \epsilon q_1(\theta) + \dots$. The parameters, obviously, must be dependent on ϵ : $\alpha = \alpha_0 + \epsilon\alpha_1 + \dots, \sigma = \sigma_0 + \epsilon\sigma_1 + \dots$. The substitution of these expressions into Equation (A33) gives the expressions for the curvature in the linear approximation, and for its derivative:

$$\begin{aligned} \kappa(s) &= 1 + \epsilon \frac{1 + 8\alpha \cos[\sqrt{1 + 8\alpha} \sigma s]}{1 + 8\alpha} + \dots, \\ \kappa'(s) &= -\epsilon \frac{8\alpha \sin[\sqrt{1 + 8\alpha} \sigma s]}{\sqrt{1 + 8\alpha}} + \dots, \end{aligned} \tag{A38}$$

where all terms of orders $\geq \epsilon^2$ are omitted.

The value of curvature at $s = 1$ must be equal to its value at $s = 0$. This implies the following condition:

$$\sqrt{1 + 8\alpha} \sigma = 2\pi n \rightarrow \alpha = \frac{4\pi^2 n^2 - \sigma^2}{8\sigma^2}. \tag{A39}$$

When $\epsilon \rightarrow 0$ (unperturbed state), parameter $\sigma \rightarrow 2\pi$. Then, $\alpha \rightarrow \alpha_0 = (n^2 - 1)/8$.

The angular coordinate $\phi(s)$ (the angle between the tangential vector and x -axis) for the contour tracing point parameterized by s is as follows:

$$\phi(s) - \phi(0) = \sigma \frac{2\pi n s (4\pi^2 n^2 + \epsilon \sigma^2)}{8\pi^3 n^3} + \frac{\epsilon (4\pi^2 n^2 - \sigma^2) \sin(2\pi n s)}{8\pi^3 n^3}. \tag{A40}$$

Recall that s changes from 0 to 1; the full length L of the contour, normalized by l , is $\sigma = L/l$, which is the ratio of the length of the contour L to the radius of the contour l measured at the point $s = 0$. Parameter $\alpha = (\omega/q_0)(l/R)^3$ determines the characteristic size of the blob as a function of the basal parameters of the state.

Using $\sigma = 2\pi + \epsilon\sigma_1 + \dots$, we find that

$$\phi(1) - \phi(0) = 2\pi + \epsilon(\frac{2\pi}{n^2} + \sigma_1). \tag{A41}$$

Obviously, $\phi(1) = \phi(0)$. Thus, the parameters σ and α take the following values:

$$\sigma = 2\pi - \epsilon \frac{2\pi}{n^2}, \quad \alpha = \frac{n^2 - 1}{8} + \frac{\epsilon}{4}, \tag{A42}$$

where $n = 2, 3 \dots$

The phase $\phi(s)$ in the considered approximation is given by the following expression:

$$\phi(s) = \frac{\pi}{2} + 2\pi s + \epsilon \frac{n^2 - 1}{n^3} \sin(2\pi ns). \tag{A43}$$

After this step in calculations, we find the following quantities:

$$\begin{aligned} v_1(s) &= -\epsilon \frac{2\pi}{n} \sin(2\pi ns), \\ v_2(s) &= -1 + \frac{\epsilon}{n^2} (1 - \cos(2\pi ns)), \end{aligned} \tag{A44}$$

and derive the contour of the vortex blob in the parametric form:

$$\begin{aligned} x(s) &= v_1(s) \cos \phi(s) - v_2(s) \sin \phi(s), \\ y(s) &= v_1(s) \sin \phi(s) + v_2(s) \cos \phi(s), \end{aligned} \tag{A45}$$

or

$$\begin{aligned} x(s) &= \rho (\cos \psi \cos \phi(s) - \sin \psi \sin \phi) = \rho \cos(\phi + \psi), \\ y(s) &= \rho (\cos \psi \sin \phi(s) + \sin \psi \cos \phi(s)) = \rho \sin(\phi + \psi), \end{aligned} \tag{A46}$$

where $\rho = \sqrt{\mu^2 + \nu^2}$ and $\psi = \arctan(\nu/\mu)$. Thus, the angle $\Phi = \phi + \psi$ determines the polar angle. In order for there to be no overlap, it is necessary that the derivative $d\Phi/ds$ is greater than zero.

Naturally, the linear approximation can only indicate the tendency. One harmonic is not enough to reveal the details of a deep contour deformation. For a more profound understanding of the problem, it is necessary to use an exact analytical solution.

On the other hand, the simple analysis that was discussed makes it possible to grasp the non-trivial fact that the parameters α and σ are not arbitrary: they are “quantized” in a certain sense. Their values are determined by integers: $n = 2, 3, \dots$. That is, if some localized area is filled with a quasi-homogeneous vortex with vorticity density q_0 , then an n -petal vortex structure can form in this area only if the parameters of this structure (size, intensity, background temperature gradient, angular velocity of disk rotation, etc.) satisfy the quantification conditions of Equation (A42). If these conditions are not met, no n -petal structure is formed at this location.

Appendix B.2. Strongly Nonlinear Configuration: Exact Analytical Solution

With the initial condition $\kappa(0) = \kappa_0$ and $\kappa_s(0) = 0$, the basal equation is

$$\begin{aligned} &\frac{1}{\sigma^2} (\kappa_s)^2 + (16\alpha\kappa_0 - \frac{1}{4}\kappa_0^4 - 8\alpha\kappa_0^2 + \\ &\frac{1}{2}\kappa_0^4) + (-16\alpha)\kappa + (8\alpha - \frac{1}{2}\kappa_0^2)\kappa^2 + \frac{1}{4}\kappa^4 = 0. \end{aligned} \tag{A47}$$

If there were no linear term in curvature κ , the periodic solution of Equation (A47) would be expressed in terms of Jacobi elliptic functions $cn(\lambda s, m)$, or $sn(\lambda s, m)$, where dimensionless parameter λ provides the periodicity of the solution: $z(0) = z(\lambda)$.

Let us bring the equation into canonical form. To do this, we will make the following manipulations: make a “shift” in κ , “flip” the result “upside down”, make a change in

magnitude, make one more “shift” in the result, and finally, make a change in magnitude again. In other words, we offer an ansatz:

$$\kappa(s) = A + \frac{B}{1 - \epsilon z(\lambda s)} \tag{A48}$$

where $z(\lambda s)$ is the Jacobi elliptic cosinus and $\lambda = n4K(m)$ for n -petal configuration: $n = 2, 3, \dots$. Parameter λ provides the periodicity of the solution ($z(0) = z(\lambda)$), i.e., the closing of the contour. Therefore, we change the argument, transitioning from σs to $\theta = \lambda s$. The first term in Equation (A47) is modified with $\sigma^{-2}(\kappa_s)^2 \rightarrow \eta^{-2}(\kappa_\theta)^2$, where $\eta = \sigma/4K(m)$.

Recall that, as is known, the elliptic cosinus satisfies the equation

$$(z')^2 + (-1 + m) + (1 - 2m)z^2 + mz^4 = 0. \tag{A49}$$

Here, prime signifies the derivative with respect to the argument. The substitution of Equation (A48) into Equation (A49) provides an equation for curvature κ , which needs to be subtracted from Equation (A47). The obtained polynomial contains six free parameters: $\alpha, \eta = \sigma/4K(m), A, B, m, \epsilon$. To zero out this polynomial, we need to zero out each of the coefficients in front of the terms with κ^l , where $l = (0 \dots 4)$. However, we have only five equations. Thus, one parameter remains free; this fixes the values of all other parameters. We select ϵ as the controlling parameter. Parameter ϵ determines the magnitude of the initial perturbation, because of $\kappa(0) = A + B/(1 - \epsilon)$. Obviously, for the unperturbed state, when $\epsilon = 0$, we have $A + B = 1, \sigma = 2\pi, m = 0, \phi(0) = \pi/2, \eta = 1$.

Omitting the details of calculations, we present the final results of these calculations:

$$\begin{aligned} A &= (-1 + 2(-1 + \epsilon^2)\mu)(\epsilon^2 + \mu - 2\epsilon^3\mu - \epsilon^4\mu + 2\epsilon(1 + \mu))/(\epsilon^2 + \mu - \epsilon^4\mu), \\ B &= 2(1 - \epsilon^2)(1 + \mu - \epsilon^2\mu)(\epsilon^2 + \mu - 2\epsilon^3\mu - \epsilon^4\mu + 2\epsilon(1 + \mu))/(\epsilon^2 + \mu - \epsilon^4\mu), \\ m &= \epsilon^2\mu, \quad \sigma = 4K(\epsilon^2\mu)\eta, \quad \alpha = (\epsilon^2 + \mu - 2\epsilon^3\mu - \epsilon^4\mu + 2\epsilon(1 + \mu))^3/8(\epsilon^2 + \mu - \epsilon^4\mu)^2, \\ \eta &= -n(-\epsilon^2 - \mu + \epsilon^4\mu)/(1 - \epsilon^2)^{1/2}(1 + \mu - \epsilon^2\mu)^{1/2}(\epsilon^2 + \mu - 2\epsilon^3\mu - \epsilon^4\mu + 2\epsilon(1 + \mu)). \end{aligned} \tag{A50}$$

Parameter $\mu(n, \epsilon)$ is fixed by the condition that the solution of equation $\sigma^{-1}\phi_s = \kappa(s)$ has to satisfy the boundary conditions $\phi(0) = \pi/2$ and $\phi(1) = 5\pi/2$. The equations obviously can be written in the following form:

$$\frac{d\phi(s)}{ds} = 4K(\epsilon^2\mu)\eta \left(A + \frac{B}{1 - \epsilon cn(n4K(\epsilon^2\mu)s, \epsilon^2\mu)} \right). \tag{A51}$$

Here, $cn(\xi, m)$ is the Jacobi elliptic cosinus, $K(m)$ is the complete elliptic integral of the first kind, $4K(0) = 2\pi, n$ is the number of petals in the vortex structure, parameters A, B and others, are taken from Equation (A50), and dimensionless parameter s changes from $s = 0$ to $s = 1$.

The calculation, which we do not present here, provides the leading term in the expansion of $\mu = \mu(n, \epsilon)$ in a series with respect to ϵ (which does not vanish when $\epsilon \rightarrow 0$): the expression $\mu \rightarrow n^2 - 1$. The graphical result of calculations for $\mu = \mu(n, \epsilon)$ is presented in Figure 5.

The expression of the blob contour is found from the following parametric representation:

$$\begin{aligned} x(s) &= v_1(s) \cos \phi(s) - v_2(s) \sin \phi(s), \\ y(s) &= v_1(s) \sin \phi(s) + v_2(s) \cos \phi(s), \end{aligned} \tag{A52}$$

where

$$v_1(s) = \frac{1}{8\alpha\eta}\kappa_s, \quad v_2(s) = -1 + \frac{1}{16\alpha\eta}\kappa_0^2 - \frac{1}{16\alpha\eta}\kappa^2. \tag{A53}$$

The graphical results of calculations of the contour shape are presented in Figure 4.

Appendix C. Model of Accretion Disk Near Black Hole

Accretion Disk: Generally speaking, different types of accretion disks are discussed in the literature: thick disks (“doughnuts”), thin disks (Shakura-Sunyaev model), slim disks, and advection-dominated accretion flows. The standard thin accretion disk model is applied for an accretion rate that is substantially smaller than the Eddington limit. This model was one of the first studies of accretion disks in the vicinity of black holes, formulated in the early 1970s by Shakura and Sunyaev. The authors articulated the basic assumptions and equations to describe classic thin disks in the Newtonian approximation of gravity. Relativistic disks were first described by Bardeen, Press, and Teukolsky, and by Novikov and Thorne. Thorne introduced the “slim disk” model, whose equations include a number of terms neglected in the thin disk model equations. For more detail, see, for example, Refs. [46,47]; these reviews cover the main aspects of the black hole accretion disk theory.

In the model presented below, the following presumptions are made about the accretion disk: (a) It is thin, i.e., its characteristic vertical thickness is much smaller than its characteristic horizontal size; (b) It is located in the equatorial plane, implying that the averaged θ -component of 4-velocity becomes suppressed; (c) It rotates with the rotation axis perpendicular to the disk plane; (d) It is heated non-homogeneously, with higher temperatures at the outer layers (due to the processes of the tidal disruption of captured matter and strong dissipation in the shear flows).

Let us assume that, due to some mechanism, a locally “twisted” region of heated matter spontaneously formed in the rotating disk. Then, in the field of the centrifugal force, within the outer layers, “hot bubbles” form (i.e., localized plasma clusters whose temperature exceeds the “average” for the disk and whose density is lower), which move *towards* the axis of the disk rotation. However, when these hot bubbles are also vorticial in nature (for example, due to the overall rotation of the disk), then each vortex bubble (via induction of the velocity field) “forces” other vortex bubbles to rotate around itself. Hence, the bubbles move “sideways”, rather than directly towards the rotation axis of the disk. As a result, since all vortices are affected by the cumulative velocity field, they gradually self-organize into zones of stability—a symmetric thermo-vorticial macro-structure which rotates as a whole around the mutual center of symmetry. The dynamics and longevity of this structure are linked to the thermal and vorticial properties of the system and its elements. Visually, the protruding components of this structure look like bright “hot petals”. For large-scale quasi-2D flows in “thin” fluid layers, with very high Reynolds numbers, the so-called “smoothing” effect is observed when the level of vorticity acquires an approximately constant value throughout the region of the vortex (see classical Ref. [26], and subsequent developments in Refs. [9,10,18,27], and references therein).

The following assumptions are also made in the model: the mass of the accretion disk ($\sim 10^{-5} \div 10^{-4} M_{BH}$) is negligible compared to the black hole “mass” M_{BH} , the radiative cooling does not strongly affect the dynamics of the fluid motion in the disk, the electrons and ions are very weakly coupled by Coulomb interaction, and therefore, ion and electron plasma components may have different temperatures, even with T_e much greater than T_i (see Ref. [28]). Then, it is the electron plasma component which contributes the most to the equation of state of the accretion disk matter. Due to the large difference in the masses of electrons and protons, electrons are highly mobile and provide the quasi-neutrality of the plasma. Also, due to the high conductivity of the plasma, its own magnetic field can be considered “frozen-in”. A range of possibilities may exist. In hot flows like those around Sgr A* or M87, electron temperature is thought to be typically lower than the ion temperature due to radiative losses to synchrotron, inverse Compton, and bremsstrahlung processes.

Model Assumptions Regarding the Thickness Of the Disk: We consider the motion of the medium relatively far from the event horizon, i.e., for hydrodynamic structures, it may be assumed that $r \gg r_g$, where r_g is the Schwarzschild radius. In this paper, the approximation $r > 3r_g$ may be considered “far away”. When we are not dealing with phenomena occurring near the event horizon (which is $r \sim r_g$), then, for $r > 3r_g$, we can

restrict ourselves to the roughest approximation for the spacetime metric near a rotating (or not) black hole.

It is assumed that the disk is geometrically thin— $h \ll r$ —where h is the characteristic local thickness of the disk.

When $r > r_g$ (more specifically, $r > 3r_g$), then the vertical component of gravity acceleration can be estimated as $g_z = -GM_{BH}z/(r^2 + z^2)^{3/2} \equiv -K^2z(1 + z^2/r^2)^{-3/2}$. This is balanced by the pressure gradient. Here, G is the gravitational constant, c is the speed of light, $K^2 = GM_{BH}/r^3 = c^2r_g/(2r^3)$, and $K \sim r^{-3/2}$ is the radius dependent on the so-called Kepler parameter: the angular velocity of a test particle with a circular orbit at a distance r from M_{BH} in the Newtonian approximation of gravity.

Gas pressure along the direction perpendicular to the disk plane (x, y) is determined by the hydrostatic equilibrium, $dP = \rho g_z dz$. Generally speaking, electromagnetic radiation and the induced magnetic field may contribute to the pressure. In the simplest case, the dominant contributor is the gas thermal pressure; then the vertical temperature distribution is isothermal, which is an acceptable approximation when the disk is optically thick and externally heated. The equation of state of gas/plasma is then $P = s^2\rho$, where s is the “isothermal sound speed” (which is not a function of the transversal coordinate z).

If we further assume that $z \ll r$, the equation of hydrostatic equilibrium becomes $s^2 d\rho = -s^2 h^{-2} \rho z dz$, the solution of which is $\rho(z) = \rho_0 \exp(-z^2/2h^2)$. Here, the transversal space scale h is introduced: $h = sr^{3/2}/(GM_{BH})^{1/2}$. Parameter ρ_0 represents the density at the disk mid-plane (at $z = 0$), and parameter h is the characteristic local thickness of the accretion disk.

In order for the accretion disk to be considered thin, it is necessary that $h/r \simeq sr^{1/2}/(GM_{BH})^{1/2} \sim (s/c)(r/r_g)^{1/2} \ll 1$. On the other hand, for great distances from the black hole ($r > r_g$), specific relativistic effects may be neglected or parametrized. Thus, we obtain the following natural bounds for the validity of our consideration: $r_g < r < r_g(c/s)^2$. In other words, the presented model may be valid for the consideration of spots in accretion disks (resembling those in Figure 1A, for example) if the spots are located within these limits.

Note that we work with the field, not with individual particles (their trajectories).

“Thin” Disk Temperature Distribution $T(r)$: The problem of how physical parameters, such as temperature, are distributed within a geometrically “thin” accretion disk may be examined, of course, within the framework of the hydrodynamical approximation, introducing, among others, the concepts of turbulent flow, Reynolds tensor, turbulent viscosity, and the closure of equations. Instead, since we are aiming to obtain only a model-specific estimate, we will first (1) neglect the dependence of physical parameters on the perpendicular to the disk-plane z -coordinate (i.e., integrate/average vertically) and (2) consider the disk without radial thermal advection (i.e., the transfer of heat with matter along the radius) and without the loss of mass from the lateral surfaces of the disk. In such a disk, the angular velocity of rotation of the disk matter at each location along the radius r is approximately equal to the angular velocity of rotation of a free test particle. In other words, $v_r \ll v_\phi$. (Recall that key parameters that determine the structure of a geometrically thin disk are the mass of the gravitating center M_{BH} , the internal radius of the accretion disk R_{in} , and the accretion rate \dot{m} .)

The next assumption is that the gas of the accretion disk spirals inward and this spiraling is very gradual, i.e., the orbits of the gas particles are almost circular. The orbital speed is Keplerian and is estimated as $v_\phi = \sqrt{GM_{BH}/r} = Kr$. Quantity $K = \sqrt{GM_{BH}/r^3}$ is the so-called Keplerian parameter, which is radially dependent, determining the period ($T_K = 2\pi/K$) of revolution of the test particle located at distance r from the center of attraction M_{BH} .

The categorization of a (vertically isothermal) disk with characteristic thickness h as “geometrically thin” means that $h/r \ll 1$, where $h^2 = 2s^2/K^2$, $s \sim \sqrt{T}$ is the isothermal sound speed for the gas, T is the absolute temperature, and the gas pressure is $p = \rho s^2$. Then, it follows from the static equilibrium for the motion in z -direction that $-dp/dz =$

$-s^2 d\rho/dz = \rho(GM_{BH}/r^2)(z/r) = \rho K^2 z$. This yields $\rho = \rho_0 \exp(-z^2/h^2)$, where ρ_0 is the density of the disk mid-plane.

The specific angular momentum of the test particle is $r v_\phi = \sqrt{GM_{BH}r}$. This means that, to flow inward (so that the radial velocity $dr/dt < 0$), the gas must lose its angular momentum by redistributing the angular momentum within the disk. The “inner” gas transfers its angular momentum to the “outer” gas; the gas matter flows inward. The loss of the angular momentum by the entire system (via the outward wind, for example) results in the inward flow of the remaining disk matter (with increased viscosity, the process becomes diffusive).

For the unit mass located at the radial distance r , the acting potential $U = -GM_{BH}/r$ produces the (inward-directed) force of attraction $f = -dU/dr = -GM/r^2$. When the mass dm is transported inward over the distance dr , its potential energy E_p is changed by $dE_p = (GM/r^2)dm dr$. The potential energy of the particle dm when moved from infinity to the location r decreases from zero to $-G dm M_{BH}/r$. One half of this energy is converted into kinetic energy; the other half is radiated away (this is the consequence of the so-called “virial theorem”). In fact, for any gravitationally bound system the time-averaged potential gravitational energy E_p and the time-averaged kinetic energy E_{kin} of the motion of the particles of the system satisfy the following condition: $E_p + 2E_{kin} = 0$. Thus, variations in the quantities are linked via the simple relationship: $\delta E_{kin} = -(1/2)\delta E_p$. Since the total energy of the disk is $E = E_{kin} + E_p = (1/2)E_p = -E_{kin}$, then $\delta E = -\delta E_{kin}$. In other words, any addition of energy to the disk reduces the kinetic energy of its particles (the disk components) and, conversely, energy radiation leads to an increase in E_{kin} , i.e., the temperature of the disk. Since one half of the variation in the gravitational energy E_p goes to the kinetic energy of the gas, then the other half is radiated. The luminosity is thus $L = (GM\dot{m}/2r^2)dr$. Divided by the radiating area, $2 \times 2\pi r \times dr$ (the first factor 2 appears because the disk has two sides), this expression produces the luminosity per unit area.

In the approximation where the disk radiates as a black body, its radiation power may be characterized by the effective temperature T (from σT^4 , where σ is the Stefan–Boltzmann constant). Equating the quantity L to the rate of energy loss via black-body radiation, we obtain $GM\dot{m}/8\pi r^3 = \sigma T^4$. When \dot{m} is presumed to be independent of the coordinate r , this expression leads to the radial temperature distribution: $T = (GM\dot{m}/8\pi\sigma r^3)^{1/4} \sim r^{-3/4}$.

This estimate was obtained for disks without radial advection (the transfer of heat with matter along the radius), without the loss of mass from the surfaces of the disk, without consideration of the boundary conditions at the inner edge of the disk, etc. For an extended source of mass (such that, within the disk, where $R_{in} < r < R$, the rate $\dot{m} = \dot{m}_0(r/R)^s$ and parameter $s > 0$)—i.e., when the inward mass transfer is balanced by the mass production at the disk periphery ($r \sim R$) and the mass is “devoured” by the black hole at the event-horizon ($r \sim R_{in}$)—the radial temperature dependence is $T \sim r^{(s-3)/4}$. This means that, depending on the value of the parameter s , the temperature curve may take various shapes. For $s = 3$, T is radius-independent (the disk is heated uniformly); no heat flow occurs along the r -direction. For $s > 3$, the disk is hotter at its periphery, where the tidal destruction of captured objects takes place.

Model of Spacetime Metrics: Obviously, equations of fluid motion in the vicinity of a black hole must be written using the concept of relativistic dynamics. In our model (see details in Refs. [29,30]), the spacetime metric is fully characterized by the black hole’s mass parameter and “spin” (for an extensive discussion, see Refs. [31–36], and the bibliographies therein). Specifically, we use the Kerr metric—an exact, singular, stationary, and axially symmetric solution of the Hilbert–Einstein equations of the gravitational “field” in a vacuum.

The notations, here and presented below, are as follows: Latin indices and suffixes take the values 0, 1, 2, 3; parameter $x^0 = ct$, c is always the speed of light; the Greek letters take the values 1, 2, 3 and correspond to the spatial coordinates. The Galilean metric (special relativity) is characterized by a metric tensor $g_{ik} = (1, -\delta_{\alpha\beta})$. For the three-

dimensional vector below, in Cartesian coordinates, there is no need to distinguish contra- and covariant components.

Using the Boyer–Lindquist four-coordinates $q^i = (t, r, \theta, \phi)$ —and it is well-known that, besides the Boyer–Lindquist coordinate representation, other representations of spacetime locations exist—the square of the interval is written as $ds^2 = g_{ik}(r/r_g, \theta)dq^i dq^k$, where notations are standard and the components of g_{ik} depend only on the dimensionless combination r_g/r and θ . Here, as accepted, $r_g = 2GM_{BH}/c^2$ is the Schwarzschild radius, c is the speed of light, G is the gravitational constant, and M_{BH} is the “mass” of the black hole. The off-diagonal term g_{03} in the metric tensor is proportional to the rate of the black hole’s own rotation and to $1/r$. We use the metric signature $diag(+ - - -)$ (see, for example, Ref. [30], and references therein). To satisfy the principle of causality for moving material objects, $ds^2 > 0$. The four timespace coordinates $q^i = (t, r, \theta, \phi)$ provide the location of a world event from the viewpoint of a remote observer. The meaning of space coordinates r, θ, ϕ is clear once transitioned to the limit $r \gg r_g, r \gg \omega r_g^2/c$. When the square of the interval becomes $ds^2 \rightarrow c^2 dt^2 - dr^2 - r^2(d\theta^2 + \sin^2\theta d\phi^2)$, i.e., at infinity, parameters r, θ, ϕ may be interpreted as the standard spherical coordinates in flat spacetime. For parameter r , strictly speaking, note that it is not the “distance”, in the usual sense, from the center of the black hole. This is because, for any material object, in the spacetime defined by equation $ds^2 = g_{ik}dq^i dq^k$, no central point $r = 0$ exists in the sense of a world event on a valid world-line.

Relativistic Flows Of Perfect Fluids: We take into account the effects of special and general relativity to obtain the relativistic Euler equations. To avoid misunderstandings that may arise due to the underdefinition of some concepts (for example, the definition of the signature of the metric tensor), we include many details in this section, even though an advanced reader will certainly be aware of them.

As is known (see, for example, Ref. [31]), the contravariant energy-momentum tensor of a perfect relativistic fluid is written as $T^{ik} = (e + p)u^i u^k - pg^{ik}$. Here, e is the internal energy of the fluid; p is the pressure. The quantity $w = e + p$ is the heat function (enthalpy); g^{ik} is the contravariant metric tensor. The quantity u^i is the contravariant 4-velocity of the fluid flow; u_i is its covariant 4-velocity. The 4-velocity vectors of the flow are normalized by the condition $u_i u^i = 1$. The covariant metric tensor (included in the definition of the interval ds via $ds^2 = g_{ik}dx^i dx^k$) is the tensor g_{ik} reciprocal to the tensor g^{ik} ; that is, $g_{il}g^{lk} = \delta^i_k$. The usual rule of summation is always used. The metric signature is chosen as $g_{00} > 0$. The procedure of the raising and lowering of these indices follows the standard rule. Therefore, the 4-vector components’ links are as follows: $u_i = g_{ik}u^k$ and $u^i = g^{ik}u_k$.

The relativistic internal energy e includes the rest energy of particles nmc^2 , where m is the rest mass of one particle and n is the proper number density of particles (i.e., $1/n$ is the volume per particle). The heat function w , normalized per mc^2 , is written as $w/mc^2 \rightarrow w = n + w_1/mc^2$. Here, w_1 captures the non-relativistic part of the heat function. Normalized pressure $p/mc^2 \rightarrow p$ has the same dimension as normalized w : $[w] = [p] = [n]$.

The explanations of why tensor T^{ik} takes such a form can be found in Ref. [12], §133. The mixed tensor T_i^k is thus $T_i^k = wu_i u^k - p\delta_i^k$. A more complex model of the stress–energy tensor of a viscous relativistic fluid with an energy flux may be found in Ref. [33], §22.3, or Ref. [12], §136. A method for building analytical models of relativistic accretion disks may also be found in Ref. [46], which also contains an extensive bibliography on the topic.

To better explain the idea of how to construct the equations of fluid motion, as the first step, we consider the flow in the flat spacetime. Then, if the Cartesian coordinates are used, $g_{00} = 1, g_{\alpha\beta} = -\delta_{\alpha\beta}$. The equations of fluid motion and the condition for the conservation of the proper number density of particles n are contained in the following equations:

$$\frac{\partial T_i^k}{\partial x^k} = 0, \quad \frac{\partial (nu^i)}{\partial x^i} = 0. \tag{A54}$$

Reminder: this system becomes closed through the inclusion of the equation of state (for the ideal gas, Fermi gas, plasma, etc.). This is the most subtle part of the problem: one

cannot just use some equation of state to “see what happens”, one must consider the real astrophysical situation in the proper spacetime for the problem. The magnetic field can also be included in the consideration. Then, tensor T_i^k would contain an additional magnetic term. If the plasma is highly conductive, then the magnetic field may be considered “frozen-in” within the fluid. Then, the additional Lorentz force appears in the dynamic equations and an additional equation for the evolution of the “frozen-in” magnetic induction \mathbf{H} appears in the system of equations. Magneto-hydrodynamics is strictly applicable in configurations when the mean free path and mean free time of electrons and protons are much smaller than the characteristic scales and time intervals of the macroscopic motions in question. However, there exist situations when, even for systems with long free paths of current-carriers, the equations obtained from the kinetic theory are formally identical to the MHD equations. Such a situation is observed, for example, in a non-equilibrium plasma when the electron temperature considerably exceeds the ion temperature.

It is physically clear that when a conducting fluid moves in a magnetic field, electric fields are induced in it. Thus, electric currents begin to flow. The magnetic field exerts forces on these currents which, in principle, may considerably modify the flow characteristics. Conversely, the currents themselves perturb and even strongly modify the magnetic field. Consequently, a complex interaction between the magnetic and fluid dynamics phenomena takes place. Thus, the fluid flow must be studied by combining the fluid dynamics equations with those of electromagnetic field equations—this is the MHD formulation. Such an approach covers a wide range of physical objects, from liquid metals in a magnetic field to cosmic plasmas. In most configurations, MHD processes are extremely complex.

The description radically simplifies if (a) all dissipative processes are neglected, i.e., no account is taken of thermal conduction and viscosity and the electrical conductivity is considered unbounded such that, in the case of a perfectly conducting fluid, the electrical field is completely screened and the magnetic field is “frozen-in” within the fluid; (b) the fluid is incompressible; (c) in the equations of conservation, the following terms are added: $H^2/8\pi$ to the density of the hydrodynamical energy $\rho v^2/2 + \rho\epsilon(\rho, \sigma)$, and the Maxwell stress tensor $-(H_\alpha H_\beta - \delta_{\alpha\beta} H^2/2)$ to the hydrodynamical momentum flux density tensor $\rho v_\alpha v_\beta + p\delta_{\alpha\beta}$. This leads to the appearance of the Lorentz force in the equation of fluid motion: $-(4\pi\rho)^{-1}[\mathbf{H}, \text{curl } \mathbf{H}]$.

The MHD formulation implies that the displacement current is neglected in the Maxwell equations, i.e., $c^{-1}|\partial_t \mathbf{E}| \ll |\text{curl } \mathbf{H}|$; together with the “frozen-in” condition, this leads to the following condition: $vl/c^2\tau \ll 1$. Here, c is the light speed, l and τ are, respectively, the characteristic space scale of the considered flow structure and of the changes in its evolution. From the Maxwell equation for the evolution of the magnetic field \mathbf{H} , which, in highly conductive plasma, becomes $\partial_t \mathbf{H} = \text{curl}[\mathbf{v}, \mathbf{H}]$, it follows that $\tau^{-1} \sim vl^{-1}$. From these two inequalities, we find that $v^2 \ll c^2$, i.e., the flow must be non-relativistic. Because $\partial_t \mathbf{v} \sim -(4\pi\rho)^{-1}[\mathbf{H}, \text{curl } \mathbf{H}]$, i.e., $\rho v/\tau \sim H^2/l$, and taking into account $vl/c^2\tau \ll 1$, we find that it must be that $H^2 \ll \rho c^2$. Thus, if the inequality $H^2 \ll \rho c_s^2 \ll \rho c^2$ (where $c_s \sim \sqrt{T}$ is the speed of sound) is satisfied, the hot plasma may be considered non-relativistic and the effect of the magnetic field can be taken into account as a small perturbation and can be neglected in the leading approximation.

With respect to the modeling of black hole accretion disks in general, one caveat is critically important: the present understanding of the physical conditions within the disks (for example, the equation of state of the matter) is highly uncertain; there are no observational measurements that confirm any of the existing models of the equation of state. Unfortunately, as all studies note, the sensitivity of numerical models to the uncertainties in the parameters of the equation of state is also high. Hence, until some reliable *observational* data appear regarding the physical conditions in the vicinity of black holes, the overzealous obsession with numerical details remains meaningless and semi-qualitative estimates will suffice.

Taking the explicit expression for T_i^k and differentiating it (using notation $\partial/\partial x_l \equiv \partial_l$), we obtain the following from Equation (A54):

$$\partial_k T_i^k = u_i \partial_k (w u^k) + w u^k \partial_k u_i - \partial_k p \delta_i^k = 0. \tag{A55}$$

We must remember that derivatives ∂_l are to be regarded as the *covariant* components of the 4-vector-operator. In fact, the differential of the scalar f , namely df , is also scalar. The scalar product of two 4-vectors, $df = dx^i \partial_i f$, is also scalar, making our assertion obvious. The operator of differentiation with respect to the coordinate, ∂_m , determines the covariant components of the 4-vector operator $\partial_l = (\partial_0, \partial_\alpha)$. The index is raised according to the usual procedure: $\partial^i = g^{ik} \partial_k$. In the Galilean metric, contravariant $\partial^l = (\partial_0, -\partial_\alpha)$, where the enumerating index for space components, as mentioned earlier, is $\alpha = 1, 2, 3$.

Next, project Equation (A55) onto the direction of the 4-velocity, i.e., we multiply it by vector u^i . This product is obviously also zero:

$$u^i u_i \partial_k (w u^k) + w u^k u^i \partial_k u_i - u^i \partial_k p \delta_i^k = 0. \tag{A56}$$

In the first term, the coefficient is $u^i u_i = 1$. The second term is zero because $u^i u_i = 1$, i.e., $u^i \partial_k u_i = 0$, and, in the Galilean metric, in the absence of the spacetime curvature, all components of the Christoffel symbol are zero. Thus,

$$\partial_k \left(\frac{w}{n} n u^k \right) - u^i \partial_i p = 0. \tag{A57}$$

(Recall that $w/c^2 = \gamma \rho + (1/c^2)(\rho e_1 + p)$, where γ is the Lorentz factor and e_1 is the non-relativistic part of the internal energy.) When we take the equation of continuity, i.e., the second equation in the system Equation (A54), into account, then Equation (A57) is transformed into

$$n u^i \left(\partial_i \left(\frac{w}{n} \right) - \frac{1}{n} \partial_i p \right) = 0. \tag{A58}$$

In the system where the total number of particles is constant and there are no external heat sources, the fundamental thermodynamical identity is $Td(s/n) = d(w/n) - (1/n)dp$. Here, T is the absolute temperature, s is the entropy per unit of proper volume, $1/n$ is the volume per particle, w is the enthalpy per unit of proper volume, and $\sigma = s/n$ is the entropy per one particle. Noting the equation of continuity, we obtain from Equation (A57) the equation of conservation for the entropy flux:

$$\partial_i (s u^i) = 0 \quad \text{or, because of } nT \neq 0, \quad u^i \partial_i \sigma = 0. \tag{A59}$$

This means there is no heat exchange between adjacent fluid particles (which are composed of enormous numbers of individual subatomic particles).

The next step is to project the first equation in Equation (A54) onto the direction perpendicular to the 4-velocity. For this, we use the projection operator, i.e., we build $(\delta_i^k - u^k u_i) \partial_l T_k^l$, which is also zero. Thus,

$$\partial_k T_i^k - u^k u_i \partial_l T_k^l = 0. \tag{A60}$$

Using the definition of T_i^k and simplifying some terms, we find four equations:

$$w u^k \partial_k u_i = \partial_i p - u^k u_i \partial_k p. \tag{A61}$$

Here, the three space components of these four equations are the relativistic generalization of Euler equations; the time component for u_0 is the consequence of the other three. Equation (A61) was obtained from Equation (A60) and the definition for T_k^l , as follows:

$$\begin{aligned} & \partial_k(wu_i u^k - p\delta_i^k) - u^k u_i \partial_l(wu_k u^l - p\delta_k^l) = \\ & \quad wu^k \partial_k u_i + u_i \partial_k(wu^k) - \partial_i p - u^k u_i \partial_l(wu_k u^l) + u^k u_i \partial_k p = \\ & wu^k \partial_k u_i + u_i \partial_k(wu^k) - \partial_i p - u^k u_i (wu^l \partial_l u_k + u_k \partial_l(wu^l)) + u^k u_i \partial_k p = \\ & wu^k \partial_k u_i + u_i \partial_k(wu^k) - \partial_i p - u^k u_i wu^l \partial_l u_k - u^k u_i u_k \partial_l(wu^l) + u^k u_i \partial_k p. \end{aligned} \tag{A62}$$

Here, the second term cancels the fifth term because $u^k u_k = 1$, and the fourth term is zero because $u^k \partial_l u_k = 0$, for the same reason; from this, we can obtain Equation (A61).

The equations of relativistic fluid dynamics in the general theory of relativity are obtained from Equations (A59) and (A61) by simply replacing the ordinary derivatives with the covariant ones (see Ref. [12], §134) and keeping in mind that the 4-velocity expression is modified as well:

$$wu^k u_{i;k} = p_{;i} - u_i u^k p_{;k}, \quad (\sigma n u^i)_{;i} = 0. \tag{A63}$$

Recall that the covariant derivatives for vectors u^i and u_i are respectively determined as $u^i_{;k} = \partial_k u^i + \Gamma_{lk}^i u^l$ and $u_{i;k} = \partial_k u_i - \Gamma_{ik}^l u_l$. The quantities of Γ_{lm}^k are the Christoffel symbols. Also, we recall that these quantities are expressed via the metric tensor g_{ik} as $\Gamma_{kl}^i = (1/2)g^{lm}(\partial_l g_{mk} + \partial_k g_{ml} - \partial_m g_{kl})$. In Galilean coordinates, Christoffel symbols $\Gamma_{lm}^k = 0$; therefore, the covariant differentiation reduces to the ordinary differentiation.

Because the covariant derivative of a scalar function produces the same result as an ordinary derivative, Equations (A63) are rewritten as

$$\begin{aligned} wu^k \partial_k u_i &= (\delta_i^k - u_i u^k) \partial_k p + wu^k \Gamma_{ik}^l u_l, \\ u^k \partial_k \sigma &= 0, \end{aligned} \tag{A64}$$

or, for a contravariant component of 4-velocity of flow u^s , the first equation becomes

$$w g_{is} u^k \partial_k u^s = (\delta_i^k - u_i u^k) \partial_k p + w(u^k \Gamma_{ik}^l g_{lm} u^m - u^m u^k \partial_k g_{im}). \tag{A65}$$

When the coordinate grid and spacetime metric are specified, then the group of the last terms in the parenthesis in Equation (A65) manifests itself as a specific “force” acting on a fluid relativistic particle in the “Euler description.” If, in analogy with the dynamics of relativistic particles with du_i/ds , we wrote, in the left part of Equation (A65), the quantity $u^k \partial_k u_i \equiv (dx^k/ds) \partial_k u_i$, this would have been incorrect. Properly, the left part should look as written in Equation (A65). The covariant quantity $u^k \partial_k u_i$ is not the specific covariant force acting on the fluid particle; this force is the quantity $g_{is} u^k \partial_k u^s$.

It is helpful to see what will happen in the case of low velocities and in the absence of fields, i.e., when $\gamma \rightarrow 1$, $u^i \rightarrow (1, \mathbf{v}/c)$, $\partial_i = (\partial_0, \partial_\alpha)$. For the α -spatial contravariant component of 4-velocity, we obtain (with the coefficient c^{-2}) the “material” derivative: $u^k \partial_k u^\alpha \rightarrow c^{-1}(\partial_t + v^\beta \partial_\beta)(v^\alpha/c) = c^{-2}(dv^\alpha/dt) \equiv c^{-2}a^\alpha$. To find the covariant component of the “material” acceleration a_α , we use the standard rule for the lowering of indices.

Thus, we become capable of calculating the spatial “force” components, using $g_{\alpha s} g^{is} = \delta_\alpha^i$, based on the following equation:

$$w g_{\alpha s} u^k \partial_k u^s = (\delta_\alpha^k - u_\alpha u^k) \partial_k p + w(u^k \Gamma_{\alpha k}^l g_{lm} u^m - u^m u^k \partial_k g_{\alpha m}), \tag{A66}$$

which has a transparent physical meaning: the left side of the equation determines the kinematic characteristics of the process—the evolution in time and space of the 4-velocity—which characterizes the state of the fluid particle; the right side of the equation specifies the causes of this change, namely, the pressure gradient and the presence of an external force field.

The subsequent calculations are conceptually rather transparent: for a given metric tensor g_{ik} found from interval ds , defined via $ds^2 = g_{ik}dx^i dx^k$, we calculate the Christoffel symbols Γ_{ij}^k ; everything is substituted into Equations (A66), which are solved for the selected model of the equation of state of (disk) matter for the quantities p, e, ϵ, σ . Equations (A66), which can be applied in many physically interesting situations, are quite complicated. The equations of fluid dynamics in the first approximation beyond the Newtonian (i.e., in the post-Newtonian, via expansion with respect to parameter c^{-2}) were obtained in Ref. [37], and are discussed in Ref. [33]. Additional information can be also found in Refs. [38–41,44].

Explicit Form of Metric Coefficients for Kerr Geometry with Rotation: For the Kerr metric (see Ref. [30] and references therein), the components of the metric tensor may be found from the following expression:

$$ds^2 = G_{00}dt^2 + G_{11}dr^2 + 2G_{03}dtd\phi + G_{22}d\theta^2 + G_{33}d\phi^2 = c^2\left(1 - \frac{r_g r}{r^2 + \hat{a}^2 \cos^2 \theta}\right)dt^2 - \left(\frac{r^2 + \hat{a}^2 \cos^2 \theta}{r^2 - r_g r + \hat{a}^2}\right)dr^2 - 2\hat{a}\left(\frac{r_g r}{r^2 + \hat{a}^2 \cos^2 \theta}\right)\sin^2 \theta dtd\phi - (r^2 + \hat{a}^2 \cos^2 \theta)d\theta^2 - (r^2 + \hat{a}^2 - \hat{a}^2 \frac{rr_g}{r^2 + \hat{a}^2 \cos^2 \theta} \sin^2 \theta)\sin^2 \theta d\phi^2. \quad (A67)$$

If we need to transition to an uniformly rotating frame of reference, then we make the following transformation $x = x_1 \cos \hat{\Omega}t - y_1 \sin \hat{\Omega}t, y = x_1 \sin \hat{\Omega}t + y_1 \cos \hat{\Omega}t, z = z_1$, where parameter $\hat{\Omega}$ is the angular velocity of the rotation co-linear with the z -axis. The same notations remain: $r \rightarrow r, \theta \rightarrow \theta, \phi \rightarrow \phi + \hat{\Omega}t$. Then,

$$ds^2 = c^2(G_{00} + 2G_{03}\hat{\Omega} + G_{33}\hat{\Omega}^2)dt^2 + G_{11}dr^2 + 2c(G_{03} + \hat{\Omega}G_{33})dtd\phi + G_{22}d\theta^2 + G_{33}d\phi^2. \quad (A68)$$

This dimensionless expression is expressed in units of length $r_g = 2GM_{BH}/c^2$ and time r_g/c . Therefore, $r \rightarrow r_g r, \hat{a} \rightarrow r_g a, \hat{\Omega} \rightarrow \Omega = \hat{\Omega}r_g/c$. Thus, Equation (A68) can be written as $ds^2 = m_{ik}dq^i dq^k$ using the following:

$$m_{00} = 1 - \frac{x}{x^2 + a^2 \cos^2 \theta} - \frac{2ax\Omega \sin^2 \theta}{x^2 + a^2 \cos^2 \theta} - \Omega^2 \frac{((x^2 + a^2)^2 - a^2(x^2 - x + a^2) \sin^2 \theta)}{x^2 + a^2 \cos^2 \theta} \sin^2 \theta, \\ m_{11} = -\frac{x^2 + a^2 \cos^2 \theta}{x^2 - x + a^2}, \quad m_{22} = -(x^2 + a^2 \cos^2 \theta), \\ m_{33} = -\frac{((x^2 + a^2)^2 - a^2(x^2 - x + a^2) \sin^2 \theta)}{x^2 + a^2 \cos^2 \theta} \sin^2 \theta, \\ m_{01} = 0, \quad m_{02} = 0, \\ m_{03} = -\frac{ax \sin^2 \theta}{x^2 + a^2 \cos^2 \theta} - \Omega \frac{((x^2 + a^2)^2 - a^2(x^2 - x + a^2) \sin^2 \theta)}{x^2 + a^2 \cos^2 \theta} \sin^2 \theta. \quad (A69)$$

As is known, for the Kerr model, the parameter is always $a^2 < 1/4$. From Equation (A69), it follows that dimensionless spacial parameter x is bounded as follows: $x_+ < x < x_{max}(\Omega, a, \theta)$ if $m_{00} > 0$. Obviously, setting $a = 0$ and $\Omega = 0$ in Equation (A69) provides the Schwarzschild metric. Also, the limit value x_+ corresponds to the external event horizon.

Finally, we provide the expressions for the components of metric tensor m_{ik} in the leading approximation for $\theta = \pi/2$, $a^2 < 1/4$ and $x \gg 1$:

$$\begin{aligned}
 m_{00} &= 1 - x^2\Omega^2 - a^2\Omega^2 - \frac{1 + 2a\Omega + a^2\Omega^2}{x}, \\
 m_{11} &= -1 - \frac{1}{x} - \frac{1 - a^2}{x^2}, \\
 m_{22} &= -x^2, \quad m_{33} = -x^2 - a^2 - \frac{a^2}{x^2}, \\
 m_{01} &= 0, \quad m_{02} = 0, \\
 m_{03} &= -x^2\Omega - a^2\Omega - \frac{a + a^2\Omega}{x}.
 \end{aligned}
 \tag{A70}$$

From these expressions, it follows that if the fluid flow is away from the event horizon (i.e., $x \gg 1 > |a|$ in dimensionless units) and parameter Ω satisfies conditions $a\Omega \ll 1$ and (approximately) $\Omega x^3 \ll 1$, then the principal contributions to the components of the metric tensor m_{ik} come from the terms which depend on Ω ; the stand-alone gravitational part in the metric is not the focal one.

The expressions in Equation (A70) make it possible to determine the size of the strip of a thin accretion disk, within which the approximation of the classical hydrodynamics can be determined, and where the main contribution to the flow dynamics is made not by the fine structure of the metric in the vicinity of a rotating black hole, but by the effect of the rotation of the accretion disk, characterized by parameter Ω . Parameter Ω appears in these expressions because the accretion disk mainly forms through the captured matter, which has a non-zero angular momentum; therefore, the (averaged) angular velocity of the disk—which is a material formation of finite mass and limited dimensions—is non-zero. Hence, it is logical to transition to a coordinate system rotating with such angular velocity. However, the very concept of a rotating coordinate system contains two implied caveats (see Ref. [31], § 84): (1) some material bodies must exist (or the coordinate system has no “anchors”) and (2) they exist within the spacetime domain, which is necessarily bound (or the material bodies outside $x_{max}(\Omega, a, \theta)$ would rotate with velocities exceeding the speed of light, which is impossible; the limit $x_{max}(\Omega, a, \theta)$ is where component m_{00} of the metric tensor turns negative). This means that a rotating coordinate system cannot extend to infinity. In other words, it is important to remember that all considerations are always made for a finite spacetime domain surrounding the axis of rotation—beyond this domain lies the “forbidden” zone. (Near the axis of rotation is the other “forbidden” zone—the ergosphere.)

As the rotation speeds up ($\Omega \rightarrow \Omega_{max}$), the “forbidden” zones (where $m_{00} < 0$) transform from two detached zones (Figure A1A) into one merged zone (Figure A1B).

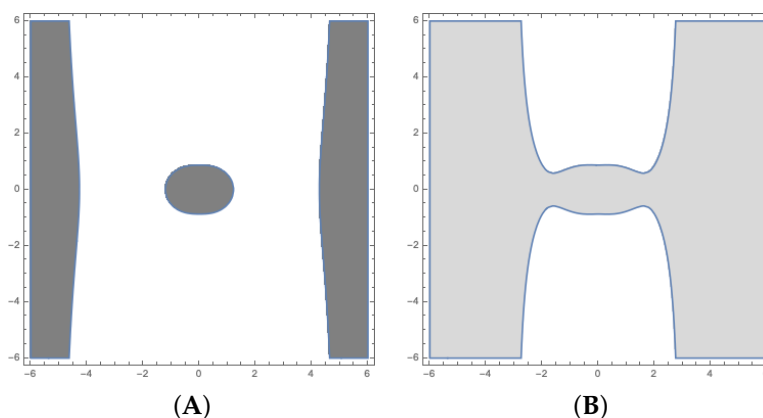


Figure A1. Domains of spacial coordinates (r, z) where the m_{00} -component of the metric tensor m_{ik} becomes negative (darkened zones). Calculations are made for the conditional values of parameters: left panel (A) $a = 1/3$, $\Omega = 1/5$; right panel (B) $a = 1/3$, $\Omega = 1/3$.

With respect to the relativistic consideration in general, several critically important caveats exist: (1) A “rigid coordinate grid” (such as the Boyer–Lindquist parametrization) cannot span everywhere, from infinity and into the ergosphere. The meanings of the parameters defining the world-point for a body do change when transitioning from one domain of spacetime into the other. This means that a “singularity” may appear. (2) The singularities of both the event horizon and the static limit in the Kerr metric are illusory. They become singularities only within the “unfortunate” choice of coordinates. Indeed, just like in the case of being far away from the black hole (at infinity) where the Boyer–Lindquist coordinates conveniently turn into normal spherical coordinates, in the case of being near the black hole, the spacetime may be smoothly described (without singularities) by differently chosen coordinates, such as Kruskal–Szekeres, Lemaitre, or Eddington–Finkelstein coordinates (see, for example, Ref. [36]). Indeed, besides the Boyer–Lindquist coordinates, a number of representations of spacetime locations exist (see, for example, Refs. [42,43]). To clarify this idea: consider the spherical coordinate system. When angular parameter $\theta = 0$ or $\theta = \pi$ (think of the North/South Poles on the globe), the contribution to the interval ds (via ds^2) from the term $\sim \sin^2 \theta d\phi^2$ always equals zero, i.e., any value of ϕ describes the same world-point (the Pole). Therefore, if working with spherical coordinates, at the Pole, we can see an illusory singularity (the ϕ -coordinate appears to “fold”). However, this is clearly a product of the “unfortunate” choice of coordinates; the “singularity” disappears in another coordinate system—in the Cartesian, for example.

Linkage Between 4-velocity and 3-velocity: To express the 4-velocities of flow u^i (in the curved spacetime with rotation) via 3-velocities, we separate the coordinates of time and space (denoted by the Greek letters) in the general form of the square of interval ds^2 :

$$ds^2 = \hat{g}_{00}(dx^0)^2 + 2g_{0\alpha}dx^0 dx^\alpha + g_{\alpha\beta}dx^\alpha dx^\beta. \tag{A71}$$

For the special case of the Kerr geometry with rotation, quantities g_{ik} are easily expressed via m_{ik} . Next, we rewrite general Equation (A71) as follows:

$$ds^2 = \hat{g}_{00}(dx^0 - g_\alpha dx^\alpha)^2 - \gamma_{\alpha\beta}dx^\alpha dx^\beta, \tag{A72}$$

where the distance dl between two close points is found from $dl^2 = \gamma_{\alpha\beta}dx^\alpha dx^\beta > 0$. Here, tensor $\gamma_{\alpha\beta} = -g_{\alpha\beta} + g_{00}g_\alpha g_\beta$ (which should not be confused with the Lorentz factor $\gamma = (1 - v^2/c^2)^{-1/2}$) includes the 3-vector \mathbf{g} whose covariant components are defined as $g_\alpha = -g_{0\alpha}/g_{00}$. Then, Equation (A72) can be rewritten as follows:

$$ds^2 = \hat{g}_{00}(dx^0 - g_\alpha dx^\alpha)^2(1 - \frac{v^2}{c^2}). \tag{A73}$$

The expression for v^2 is apparent from Equations (A72) and (A73) and reveals that, in order to measure the magnitude of flow velocity v , one must simultaneously measure the distance between neighboring points dl (in Equation (A72)) and the interval of the corresponding time. This is why the expression $\sqrt{\hat{g}_{00}}(dx^0 - g_\alpha dx^\alpha)$ is introduced.

From Equation (A73), it follows that

$$\frac{dx^0}{ds} \equiv u^0 = \frac{\gamma}{\sqrt{\hat{g}_{00}}} + g_\beta u^\beta. \tag{A74}$$

The link between the components of the general tensor g_{ik} and the components of the specific case of the Kerr metric with rotation m_{ik} is given by the following:

$$\begin{aligned} \hat{g}_{00} &\rightarrow m_{00}, & g_{11} &\rightarrow m_{11}, & g_{22} &\rightarrow m_{22}, & g_{33} &\rightarrow m_{33}, \\ g_{01} &\rightarrow 0, & g_{02} &\rightarrow 0, & g_{03} &\rightarrow m_{03}. \end{aligned} \tag{A75}$$

Tensor $\gamma_{\alpha\beta}$, introduced in Equation (A73), becomes, in this cas, $\gamma_{\alpha\beta} \rightarrow -m_{\alpha\beta} + g_\alpha g_\beta m_{00}$. It should be noted that tensor $\gamma_{\alpha\beta}$ determines the metric in 3D space: the distance

between two close points can be found from $dl^2 = \gamma_{\alpha\beta} dx^\alpha dx^\beta$. The contravariant 3D metric tensor is $\gamma^{\alpha\beta} = -g^{\alpha\beta}$ (see Ref. [31], §84). Also, when $g_\alpha = -g_{0\alpha}/\hat{g}_{00}$, the contravariant component of the same vector \mathbf{g} is determined as follows: $g^\alpha = \gamma^{\alpha\beta} g_\beta = -g^{0\alpha}$. We can also obtain that $\hat{g}^{00} = \hat{g}_{00}^{-1} - g_\alpha g^\alpha$.

Synchronized Time: The introduction of parameter z^0 defined by $dz^0 = \sqrt{\hat{g}_{00}}(dx^0 - g_\alpha dx^\alpha)$ —the so-called *synchronized time*—is not some kind of mathematical manipulation. It reflects the fundamental need within the framework of relativism to simultaneously measure positions at two separate points and, therefore, to measure the particle velocity. This means that the measured time interval is $\sqrt{\hat{g}_{00}}(dx^0 - g_\alpha dx^\alpha)$, divided by c ; the concept of the velocity of fluid particle movement is formulated using this very time interval. Equation (A71) allows us to conclude that 3D contravariant and covariant velocities take the following form:

$$v^\alpha = \frac{cdx^\alpha}{\sqrt{\hat{g}_{00}}(dx^0 - g_\beta dx^\beta)} = \frac{cu^\alpha}{\sqrt{\hat{g}_{00}}(u^0 - g_\beta u^\beta)},$$

$$v_\alpha = \gamma_{\alpha\beta} v^\beta, \quad v_\alpha v^\alpha = v^2. \tag{A76}$$

Furthermore, from Equations (A75) and (A76), the contravariant components of 4-velocity are not introduced arbitrarily, but, following the procedure above, are expressed via the 3-velocity vector \mathbf{v} as follows:

$$u^i = \frac{dx^i}{ds} = (u^0, u^\alpha) = \left(\frac{\gamma}{\sqrt{\hat{g}_{00}}} + \gamma \frac{g_\alpha v^\alpha}{c}, \gamma \frac{v^\alpha}{c} \right). \tag{A77}$$

Equation (A77) provides the link between the 4-velocities u^i and 3-vectors of flow velocities v^α . Note that, in this case, the operator $u^k \partial_k$ can be written as $\equiv (\gamma/c)D$, where $D = \partial_{t_0} + v^\beta \partial_\beta$ and $t_0 = z_0/c$. In fact,

$$u^k \partial_k = \gamma \left(\left(\frac{1}{\sqrt{\hat{g}_{00}}} + g_\beta \frac{v^\beta}{c} \right) \partial_0 + \frac{v^\beta}{c} \partial_\beta \right) = \gamma \left(\left(\frac{dz_0}{\sqrt{\hat{g}_{00}} dz_0} + \frac{g_\alpha dx^\alpha}{dz_0} \right) \partial_0 + \frac{v^\beta}{c} \partial_\beta \right) =$$

$$\gamma \left(\left(\frac{dz_0 + \sqrt{\hat{g}_{00}} g_\alpha dx^\alpha}{\sqrt{\hat{g}_{00}} dz_0} \right) \partial_0 + \frac{v^\beta}{c} \partial_\beta \right) = \gamma \left(\left(\frac{\sqrt{\hat{g}_{00}} dx^0}{\sqrt{\hat{g}_{00}} dz_0} \right) \partial_0 + \frac{v^\beta}{c} \partial_\beta \right) = \gamma \left(\frac{\partial}{\partial z^0} + \frac{v^\beta}{c} \partial_\beta \right) = \frac{\gamma}{c} D.$$

Thus, the operator D is nothing more than a “material” derivative with respect to time, in which, instead of differentiation with respect to the time t of a remote observer, differentiation with respect to synchronized time $t_0 = z_0/c$ is implied.

“Specific Force” and Coriolis Effect: Let us return to Equation (A65), which we write using the following form:

$$wg_{\beta s} u^k \partial_k u^s = (\delta_\beta^k - u_\beta u^k) \partial_k p + w f_\beta, \tag{A78}$$

where, after some simple manipulations, f_β becomes a remarkably symmetric expression

$$f_\beta = \frac{1}{2} (\partial_\beta g_{km} - \partial_k g_{\beta m} - \partial_m g_{\beta k}) u^m u^k. \tag{A79}$$

The term f_i in Equation (A78) is non-zero in a curved spacetime and manifests itself as a certain specific force acting on a moving fluid particle.

The key question that immediately arises is whether Equation (A78) provides similar expressions to the centrifugal and Coriolis forces which appear in the classical hydrodynamics.

We expand the expression for f_β , explicitly selecting terms with u^0 :

$$f_\beta = \frac{1}{2}(\partial_\beta g_{00})(u^0)^2 + \left[(\partial_\beta g_{\lambda 0} - \partial_\lambda g_{\beta 0})u^0 \right] u^\lambda + \frac{1}{2}(\partial_\beta g_{\mu\nu} - \partial_\mu g_{\nu\beta} - \partial_\nu g_{\beta\mu})u^\mu u^\nu. \tag{A80}$$

The first term in Equation (A80) can be rewritten as follows:

$$\frac{1}{2}(\partial_\beta g_{00})(u^0)^2 = \frac{1}{2g_{00}}(\partial_\beta g_{00})(1 + \gamma \frac{\sqrt{g_{00}}g_\alpha v^\alpha}{c})^2 = (\partial_\beta \ln \sqrt{g_{00}})(1 + \gamma \frac{\sqrt{g_{00}}g_\alpha v^\alpha}{c})^2. \tag{A81}$$

Indeed, this expression turns into the simple model of Newtonian gravity in the limit case of the weak field, non-rotation of the black hole, and when the very last term is zero. This last term reflects the combined effect of the rotation of “everything” (via g_α), movement (via v^α/c), and gravity (via g_{00}).

We rewrite the second term in Equation (A80) as follows:

$$(\partial_\beta g_{\lambda 0} - \partial_\lambda g_{\beta 0})u^0 u^\lambda = (\delta_\beta^\mu \delta_\lambda^\nu - \delta_\beta^\nu \delta_\lambda^\mu) \partial_\mu g_{\nu 0} u^0 u^\lambda = u^0 \sqrt{d} \epsilon_{\beta\lambda\sigma} u^\lambda \left(\frac{\epsilon^{\mu\nu\sigma}}{\sqrt{d}} \partial_\mu g_{\nu 0} \right). \tag{A82}$$

Here, in a system with the right orientation of basis vectors, the Levi–Civita symbol $\epsilon^{\mu\nu\lambda}$ (recall that this is not a tensor) has the components $\epsilon^{123} = \epsilon_{123} = 1$, and its sign changes when index transposition is not even. In curvilinear 3D coordinates, the unit antisymmetric tensor is defined as $\kappa_{\alpha\beta\gamma} = d^{1/2} \epsilon_{\alpha\beta\gamma}$, where d is the determinant of the matrix of the metric tensor $g_{\mu\nu}$. Respectively, the tensor $\kappa^{\alpha\beta\gamma} = d^{-1/2} \epsilon^{\alpha\beta\gamma}$. The expression in parentheses in Equation (A82), i.e., $\kappa^{\alpha\beta\gamma} \partial_\mu g_{\nu 0}$, is σ -component of the 3D contravariant vector $\Gamma = (\text{curl}(-g_{00}\mathbf{g}))^\sigma$ (see Ref. [48]; or Ref. [31], footnote on p. 252). In combination with other multipliers, Equation (A82) produces the cross-product of vectors \mathbf{v} and Γ with coefficient $\gamma u^0/c$. Indeed, if $\mathbf{c} = \mathbf{a} \times \mathbf{b}$, then $c_\alpha = \kappa_{\alpha\beta\gamma} a^\beta b^\gamma$. Thus, the second term in Equation (A80) can be written as $\gamma u^0 c^{-1} [\mathbf{v} \times \text{curl}(-g_{00}\mathbf{g})]$, in accordance with the definition of the cross-product in 3D curvilinear coordinates. The second term in Equation (A80) has an analogous form (absent external fields) to the Coriolis specific force that would appear in a frame rotating with angular velocity $\Omega = (c/2)\gamma u^0 \text{curl}(-g_{00}\mathbf{g})$.

In the limit case of low velocities and in the absence of fields (i.e., when $\gamma \rightarrow 1, u^0 \rightarrow 1, \sqrt{d} \rightarrow x, g_{\nu 0} \rightarrow -\Omega x^2, \partial_\mu \rightarrow \partial_1$), the non-zero component of Ω , i.e., Ω^θ , becomes $(1/2)\epsilon^{132} x^{-1} \partial_1(-\Omega x^2) = \Omega$, which is the angular velocity of the rotation of the coordinate system. In this case, Equation (A82) becomes $2\epsilon_{\beta\lambda 2} x u^\lambda \Omega$, i.e., we can obtain the expression for the Coriolis force in spherical coordinates, with the presence of coefficients 2 and Ω . Recall that, in the full expression for the radial component of the cumulative “force,” the following terms are summarized: the radial component of the Coriolis force ($\sim 2x\dot{\phi}\Omega$), the radial component of the centrifugal force ($\sim x\Omega^2$), and the term ($\sim x\dot{\phi}^2$) from the material derivative for the flow velocity. By summing up, we can obtain the radial component $\sim x(\Omega + \dot{\phi})^2$.

The third term—which provides the relativistic correction to the leading terms in Equation (A80)—appears due to both the large flow velocities and the curvature of space-time. This term is present when the derivatives with respect to the 3-coordinates of the spatial part of the metric tensor, $g_{\mu\nu}$, are non-zero. After the substitution $g_{\alpha\beta} = -\gamma_{\alpha\beta} + g_{00}g_\alpha g_\beta$, some of the terms are canceled, and the remaining ones contribute to the Christoffel symbol over a spatial basis. In Cartesian coordinates, this term disappears.

Each term in Equation (A80) is drastically simplified in the case of low ($v^2 \ll c^2$) fluid flow velocities, i.e., when $\gamma \simeq 1$ and when $c \gg \sqrt{g_{00}}g_\alpha v^\alpha$: the first term in f_β is then

transformed into a specific potential “force” (acting on a fluid particle of flow) which is a strictly radial one in the case of the Schwarzschild metric. In the case of the Kerr metric, this term includes both the “gravitational” action and the “centrifugal” effect dependent on Ω^2 and a^2 (see m_{00} in Equation (A69)). The second term, as noted above, is analogous to the Coriolis force in the classic hydrodynamics. The third term is negligible for low flow velocities.

The subsequent simplification of Equation (A80) involves the expansion of all dynamic quantities into series with respect to small parameters x^{-1} and v^2/c^2 , which produces rather cumbersome expressions. The contribution to the equation of fluid motion from the terms containing the higher orders of flow velocity \mathbf{v} will be negligible. The key difference compared to the classic hydrodynamic treatment is the replacement of the classic gravity acceleration $-\nabla\Phi$ with $-\nabla\ln\sqrt{m_{00}}$ and the replacement of the classic angular velocity Ω with parameter Ω , as written above.

If conditions $x \gg 1$, $\Omega x < 1$ are satisfied, then, leaving the leading terms in the expansion $\partial_\beta \ln \sqrt{m_{00}}$, we obtain that $\partial_\beta \ln \sqrt{m_{00}} \simeq -x\Omega^2 + 1/2x^2 + 1/2x^3 + (2a + \Omega)\Omega/2x^2$. Here, terms of a higher order of smallness are omitted. The first term describes the centrifugal effect, the second describes the contribution of the force of attraction in the Newtonian approximation of gravity, the third term is derived from the Schwarzschild model of non-rotating black holes, the last term takes into account the rotation of both the black hole and the disk. For $x \gg 1$, $\Omega x < 1$, but $\Omega x^{3/2} > 1/2$, the principal contribution provides the first term $\sim \Omega^2$, i.e., the centrifugal effect, independently of the exact structure of the spacetime near the rotating, or not rotating, black hole.

Derivation of Equations for Relativistic Flow: In the subsequent treatment, the following expressions are useful. For a 3-vector \mathbf{a} with covariant components a_α , the contravariant components of vector $\text{curl } \mathbf{a}$ are $(\text{curl } \mathbf{a})^\alpha = 2^{-1}(d)^{-1/2}\epsilon^{\alpha\beta\gamma}(\partial_\beta a_\gamma - \partial_\gamma a_\beta)$. Also, $\text{div } \mathbf{a} = (d)^{-1/2}\partial_\alpha(d^{1/2}a^\alpha)$. When the fluid can be considered “incompressible”, the current potential A^μ may be introduced: $v^\alpha = d^{-1/2}\epsilon^{\alpha\mu\nu}\partial_\mu A_\nu$.

By rearranging the terms, we rewrite Equation (A78) in the following form:

$$\begin{aligned}
 & -wg_{\beta\alpha}\frac{\gamma}{c}D\frac{\gamma v^\alpha}{c} - 2\frac{\gamma w}{c^2}[\mathbf{v} \times \boldsymbol{\Omega}]_\beta - \partial_\beta p - w\frac{1}{2}(\partial_\beta g_{00})(u^0)^2 = \\
 & -u_\beta\frac{\gamma}{c}Dp - wg_{\beta 0}\frac{\gamma}{c}Du^0 + w\frac{\gamma^2}{2c^2}(\partial_\beta g_{\mu\nu} - \partial_\mu g_{\nu\beta} - \partial_\nu g_{\beta\mu})v^\mu v^\nu.
 \end{aligned}
 \tag{A83}$$

Remember here that (for the spacial components) $u^\nu = \gamma v^\nu/c$ and $u_\nu = -\gamma v_\nu/c$.

Presuming that the metric tensor components g_{00} and $g_{\alpha\beta}$ are time-independent, when low-velocity flows ($v^2 \ll c^2$, i.e., $\gamma \rightarrow 1$ and $w \rightarrow \gamma c^2 \rho \rightarrow c^2 \rho$) are considered at some distance from the event horizon (i.e., $(u^\alpha)^2 \Gamma \ll 1$, where Γ is a characteristic magnitude of the Christoffel symbols), then the right side in Equation (A83) may be dropped. On the other hand, the thermodynamical quantity $p = p(n, \sigma)$ gives $(u^k \partial_k)p = (\partial p/\partial n)_s(u^k \partial_k)n + (\partial p/\partial \sigma)_n(u^k \partial_k)\sigma$. For low velocities, $u^0 \rightarrow (g_{00})^{-1/2}$, and the last term on the left side of Equation (A83) becomes $w\partial_\beta \ln \sqrt{g_{00}}$. The equation for the evolution of flow velocities then becomes:

$$-\frac{w}{c^2}Dv_\beta - 2\frac{w}{c^2}[\mathbf{v} \times \boldsymbol{\Omega}]_\beta = \partial_\beta p + w\partial_\beta \ln \sqrt{g_{00}} + \dots
 \tag{A84}$$

The simplest formulation is the one made in the Cartesian coordinates. Then, we may not distinguish between the contra- and covariant components of a vector and simply write the following: $v^\alpha = v_\alpha = \epsilon_{\alpha\mu\nu}\partial_\mu A_\nu$ and $(\text{curl } \mathbf{v})_\alpha = \epsilon_{\alpha\beta\gamma}\partial_\beta v_\gamma = \epsilon_{\alpha\beta\gamma}\partial_\beta(\epsilon_{\gamma\mu\nu}\partial_\mu A_\nu) = \epsilon_{\alpha\beta\gamma}\epsilon_{\gamma\mu\nu}\partial_\beta\partial_\mu A_\nu = (\delta_{\mu\alpha}\delta_{\nu\beta} - \delta_{\nu\alpha}\delta_{\mu\beta})\partial_\beta\partial_\mu A_\nu$. So, $(\text{curl } \mathbf{v})_\alpha = \partial_\alpha(\partial_\mu A_\mu) - \partial_\nu\partial_\nu A_\alpha = -\Delta A_\alpha$ when $\partial_\mu A_\mu = 0$ (for example, when there is only one component of the vector $A_\mu \rightarrow (0, 0, A_3(q^1, q^2))$, which is not dependent on the polar coordinate $q^3 \equiv \phi$). Here, Δ is the Laplace operator.

2D Flows: Consider the flow in a thin layer of an ideal fluid in the plane $\theta = \pi/2$. In this case, the flow velocity v_α has only two non-zero components in the xy -plane. Then,

$\omega = \text{curl } \mathbf{v}$ (in terms of components: $\omega_\lambda = \epsilon_{\lambda\mu\nu} \partial_\mu v_\nu$) has only one non-zero component $A_3 \equiv \psi$, i.e., ω_3 is perpendicular to the xy -plane.

We assume that a state of dynamical equilibrium exists:

$$\partial_\beta p_s + \rho_0 \partial_\beta \ln \sqrt{g_{00}} = 0. \tag{A85}$$

We will now write $p = p_s + p_1$, $\rho = \rho_0 + \rho_1$. Combining Equation (A85) with Equation (A84), we find that a perturbed state is described by the following:

$$-\rho_0(Dv_\beta + 2[\mathbf{v} \times \boldsymbol{\Omega}]_\beta) = \partial_\beta p_1 + \rho_1 \partial_\beta \ln \sqrt{g_{00}}. \tag{A86}$$

In this equation, the small term $\sim \rho_1 Dv_\beta$ is omitted for similar reasons to those articulated in Refs. [12], §13, or [14]: We suppose that the space-scale of structures which are of interest to us is small in comparison with the distances over which the force-field from m_{00} causes a noticeable change in density, and we can regard the fluid itself as incompressible. This means that, during this process, we can neglect the change in the density caused by the pressure change. The change in density caused by thermal expansion, $\rho_1 \simeq (\partial\rho/\partial T)_p(T - T_0)$, cannot be neglected, because this is the one which causes the phenomenon.

All the necessary attributes in the evolution equation Equation (A86) are presented: on the left is the kinematic quantity, which is dependent on the flow velocity \mathbf{v} , which describes the change in the state of the fluid particle in the Euler description, and on the right are the terms characterizing the causes which drive this change—the gradient pressure and the force characteristic determined by the metric coefficient m_{00} .

Next, the following well known expressions are used: $(\mathbf{v} \cdot \nabla)\mathbf{v} = \nabla(v^2/2) - [\mathbf{v} \times \boldsymbol{\omega}]$, where $\boldsymbol{\omega} = [\nabla \times \mathbf{v}]$ and $[\nabla \times [\mathbf{A} \times \mathbf{B}]] = (\mathbf{B} \cdot \nabla)\mathbf{A} - (\nabla \cdot \mathbf{A})\mathbf{B} + (\nabla \cdot \mathbf{B})\mathbf{A} - (\mathbf{A} \cdot \nabla)\mathbf{B}$ which provide $[\nabla \times [\mathbf{v} \times \boldsymbol{\omega}]] = (\boldsymbol{\omega} \cdot \nabla)\mathbf{v} - (\nabla \cdot \mathbf{v})\boldsymbol{\omega} + (\nabla \cdot \boldsymbol{\omega})\mathbf{v} - (\mathbf{v} \cdot \nabla)\boldsymbol{\omega}$. Then, we can move forward. Next, we have $\text{div } \mathbf{v} = 0$. Obviously, $\text{div } \boldsymbol{\omega} = 0$. In this case, for 2D flows in the xy plane, $\text{curl}[\mathbf{v} \times \boldsymbol{\omega}] = -(\mathbf{v} \cdot \nabla)\boldsymbol{\omega}$. Full vorticity can be determined as $-\Delta\psi + 2\boldsymbol{\Omega}$. The evolution equation, Equation (1), for function ψ (in $v_\beta = \epsilon_{\beta\mu 3} \partial_\mu \psi$) is found after some manipulations, excluding $\partial_\beta p_1$ using the operation $\epsilon_{\gamma\beta\alpha} \partial_\alpha \partial_\beta p_1$.

The condition $\text{div } \mathbf{v} = 0$ does not mean that the density of the medium is constant. This condition simply means that the density evolution takes place according to the following equation: $D\rho = 0$. Using $\rho = \rho_0 + (\partial\rho/\partial T)_p(T - T_0) + (\partial\rho/\partial p)_T(p - p_0) \simeq \rho_0(1 - \beta_p(T - T_0))$, after some simple manipulation, the evolution equation for temperature perturbations takes the form of the third equation in Equation (1). For the equation of state we shall assume, in accordance with the assumption of $\text{div } \mathbf{v} \rightarrow 0$, that the density essentially depends only on the temperature and not on the pressure. Thus, we set $\rho = \rho_0(1 - \beta_p(T - T_0))$, where subscript 0 denotes the reference values. The coefficient of thermal expansion β_p is presumed constant. Since the quantity $\beta_p(T - T_0)$ is generally small, one may neglect the density variations, and hence replace ρ with the constant value ρ_0 in all terms, except in the “buoyancy” term.

Condition $\text{div } \mathbf{v} = 0$ is not merely wishful. This condition is applicable in situations where, on the one hand, the magnitude of the instantaneous current velocity v may be considered small compared to the speed of sound s , i.e., $v^2 \ll s^2$, and, on the other hand, the time τ during which the flow configuration changes meaningfully is large compared to the time which is necessary for the sound signal to travel distances of the order of the size l of the vortical structure in the flow, i.e., $\tau \gg l/s$ (see Ref. [12]). Then, we can assume that information about the disturbance of the medium is transmitted by an acoustic signal, as if instantly, i.e., the medium can be considered incompressible. Obviously, the requirement must also be met that the speed of sound s , although large compared to the value of the local current velocity in the medium, must be less than the speed of light c .

Condition $\text{div } \mathbf{v} = 0$ means that the flow velocity \mathbf{v} is uniquely determined by specifying the vorticity $\boldsymbol{\omega} = \text{curl } \mathbf{v}$. Indeed, from the well known identity $\text{curl } \text{curl } \mathbf{b} = \nabla \text{div } \mathbf{b} - \Delta \mathbf{b}$ for any vector quantity \mathbf{b} , it follows that when $\text{div } \mathbf{v} = 0$, then $\Delta \mathbf{v} = -\text{curl } \boldsymbol{\omega}$,

and, consequently, $\mathbf{v} = -\text{curl} \int d\mathbf{x}_1 G(\mathbf{x} - \mathbf{x}_1) \omega(\mathbf{x})_1$. Here, $G(\mathbf{x} - \mathbf{x}_1)$ is the Green function of the problem $\Delta G(\mathbf{x} - \mathbf{x}_1) = \delta(\mathbf{x} - \mathbf{x}_1)$ with boundary conditions. The final remark is that since the velocity is determined through the integral of the product of the vorticity q and the Green's function G , even if the model vorticity distribution function is chosen to be “bumpy”, the integration process—smoothing—produces a resulting function that is “smooth”, i.e., the function is “well-defined” and correctly (at least qualitatively) describes the examined process.

References

1. Akiyama, K.; Alberdi, A.; Alef, W.; Algaba, J.C.; Anantua, R.; Asada, K.; Azulay, R.; Bach, U.; Baczko, A.K.; Ball, D.; et al. First Sagittarius A* Event Horizon Telescope Results. I. The Shadow of the Supermassive Black Hole in the Center of the Milky Way. *Astrophys. J. Lett.* **2022**, *930*, L12. [[CrossRef](#)]
2. Akiyama, K.; Alberdi, A.; Alef, W.; Algaba, J.C.; Anantua, R.; Asada, K.; Azulay, R.; Bach, U.; Baczko, A.K.; Ball, D.; et al. First Sagittarius A* Event Horizon Telescope Results. II. EHT and Multiwavelength Observations, Data Processing, and Calibration. *Astrophys. J. Lett.* **2022**, *930*, L13. [[CrossRef](#)]
3. Akiyama, K.; Alberdi, A.; Alef, W.; Algaba, J.C.; Anantua, R.; Asada, K.; Azulay, R.; Bach, U.; Baczko, A.K.; Ball, D.; et al. First Sagittarius A* Event Horizon Telescope Results. III. Imaging of the Galactic Center Supermassive Black Hole. *Astrophys. J. Lett.* **2022**, *930*, L14. [[CrossRef](#)]
4. Akiyama, K.; Alberdi, A.; Alef, W.; Algaba, J.C.; Anantua, R.; Asada, K.; Azulay, R.; Bach, U.; Baczko, A.K.; Ball, D.; et al. First Sagittarius A* Event Horizon Telescope Results. IV. Variability, Morphology, and Black Hole Mass. *Astrophys. J. Lett.* **2022**, *930*, L15. [[CrossRef](#)]
5. Akiyama, K.; Alberdi, A.; Alef, W.; Algaba, J.C.; Anantua, R.; Asada, K.; Azulay, R.; Bach, U.; Baczko, A.K.; Ball, D.; et al. First Sagittarius A* Event Horizon Telescope Results. V. Testing Astrophysical Models of the Galactic Center Black Hole. *Astrophys. J. Lett.* **2022**, *930*, L16. [[CrossRef](#)]
6. Akiyama, K.; Alberdi, A.; Alef, W.; Algaba, J.C.; Anantua, R.; Asada, K.; Azulay, R.; Bach, U.; Baczko, A.K.; Ball, D.; et al. First Sagittarius A* Event Horizon Telescope Results. VI. Testing the Black Hole Metric. *Astrophys. J. Lett.* **2022**, *930*, L17. [[CrossRef](#)]
7. NASA/JPL-Caltech/SwRI/ASI/INAF/JIRAM, Cyclones Encircle Jupiter's North Pole. Available online: <https://www.jpl.nasa.gov/images/pia22335-cyclones-encircle-jupiters-north-pole> (accessed on 19 August 2023).
8. NASA's Earth Observatory, The Antarctic Ozone Hole in 2002. Available online: <https://earthobservatory.nasa.gov/images/2832/the-antarctic-ozone-hole-in-2002> (accessed on 19 August 2023).
9. Goncharov, V.P.; Pavlov, V.I. Hamiltonian contour dynamics. In *Fundamental and Applied Problems of the Vortex Theory*; Borisov, A.V., Mamaev, I.S., Sokolovskiy, M.A., Eds.; Institute of Computer Science: Moscow–Izhevsk, Russia, 2003; pp. 179–237. (In Russian)
10. Goncharov, V.P.; Pavlov, V.I. *Hamiltonian Vortex and Wave Dynamics*; Geos: Moscow, Russia, 2008.
11. Akiyama, K.; Alberdi, A.; Alef, W.; Algaba, J.C.; Anantua, R.; Asada, K.; Azulay, R.; Bach, U.; Baczko, A.K.; Ball, D.; et al. First Sagittarius A* Event Horizon Telescope Results. VII. Polarization of the Ring. *Astrophys. J. Lett.* **2024**, *964*, L25. [[CrossRef](#)]
12. Landau, L.D.; Lifshitz, E.M. *Fluid Mechanics*, 2nd ed.; Pergamon Press: Oxford, NY, USA, 1987.
13. Milne-Thomson, L.M. *Theoretical Hydrodynamics*, 5th ed.; MacMillan: London, UK, 1968.
14. Turner, J.S. *Buoyancy Effects in Fluids*; Cambridge University Press: Cambridge, UK, 1979.
15. Runge, J.; Walker, S.A. Probing within the Bondi radius of the ultramassive black hole in NGC 1600. *arXiv* **2021**, arXiv:2102.06216.
16. Wong, K.-W.; Irwin, J.A.; Yukita, M.; Million, E.T.; Mathews, W.G.; Bregman, J.N. Resolving the Bondi accretion flow toward the supermassive black hole of NGC 3115 with *Chandra*. *Astrophys. J. Lett.* **2011**, *736*, L23. [[CrossRef](#)]
17. Tito, E.P.; Goncharov, V.P.; Pavlov, V.I. Hot Spots in Sgr A* Accretion Disk: Hydrodynamic Insights. *Universe* **2023**, *9*, 40. [[CrossRef](#)]
18. Goncharov, V.P.; Gryanik, V.M.; Pavlov, V.I. Venusian “hot spots”: Physical phenomenon and its quantification. *Phys. Rev. E* **2002**, *66*, 066304. [[CrossRef](#)] [[PubMed](#)]
19. Madelung, E. *Die Mathematischen Hilfsmittel des Physikers*; Springer: Gottingen, Germany; Berlin/Heidelberg, Germany, 1957.
20. Abramowitz, M.I.; Stegun, I.A. *Handbook of Mathematical Functions: With Formulas, Graphs, and Mathematical Tables*; United States Government Printing Office: Washington, DC, USA, 1972.
21. Kovacic, I.; Brennan, M.J. *The Duffing Equation: Nonlinear Oscillators and Their Behaviour*; John Wiley & Sons: Hoboken, NJ, USA, 2011.
22. Rand, R.H. *Lecture Notes on Nonlinear Vibrations*; Cornell University: Ithaca, NY, USA, 2012.
23. Abramowicz, M.; Lanza, A.; Spiegel, E.; Szuszkiewicz, E. Vortices on accretion disks. *Nature* **1992**, *356*, 41–43. [[CrossRef](#)]
24. Tursunov, A.; Zajaček, M.; Eckart, A.; Kološ, M.; Britzen, S.; Stuchlík, Z.; Czerny, B.; Karas, V. Effect of Electromagnetic Interaction on Galactic Center Flare Components. *Astrophys. J.* **2020**, *897*, 99. [[CrossRef](#)]
25. Kundu, P.K.; Cohen, I.M.; Dowling, D.R. *Fluid Mechanics*; Academic Press: Cambridge, MA, USA, 2015.
26. Lavrent'ev, M.A.; Shabat, B.V. *Hydrodynamic Problems and Their Mathematical Models*; Nauka: Moscow, Russia, 1973.
27. Goncharov, V.P.; Pavlov, V.I. *Problemy Gidrodinamiki v Gamil'tonovom Opisani*; Izd-vo Moskovskogo Universiteta: Moskva, Russia, 1993.
28. Kadomtsev, B.B. *Collective Phenomena in Plasma*, 2nd ed.; Nauka: Moscow, Russia, 1988.

29. Tito, E.P.; Pavlov, V.I. Relativistic Motion of Stars near Rotating Black Holes. *Galaxies* **2018**, *6*, 61. [[CrossRef](#)]
30. Tito, E.P.; Pavlov, V.I. Black Hole Spin and Stellar Flyby Periastron Shift. *Universe* **2021**, *7*, 364. [[CrossRef](#)]
31. Landau, L.D.; Lifshitz, E.M. *The Classical Theory of Fields*; Elsevier: Amsterdam, The Netherlands, 2013.
32. Weinberg, S. *Gravitation and Cosmology: Principles and Applications of the General Theory of Relativity*; Wiley: New York, NY, USA, 1972.
33. Misner, C.W.; Thorne, K.S.; Wheeler, J.A. *Gravitation*; W.H. Freeman and Company, Princeton University Press: Princeton, NJ, USA, 1973.
34. Shapiro, S.L.; Teukolsky, S.A. *Black Holes, White Dwarfs, and Neutron Stars*; Wiley: Hoboken, NJ, USA, 1983. [[CrossRef](#)]
35. Visser, M. The Kerr Spacetime: A Brief Introduction. *arXiv* **2008**, arXiv:0706.0622v3.
36. Frolov, V.P.; Zelnikov, A. *Introduction to Black Hole Physics*; Oxford University Press: Oxford, UK, 2011.
37. Chandrasekhar, S. The post-newtonian equations of hydrodynamics in general relativity. *Astrophys. J.* **1965**, *142*, 1488–1512. [[CrossRef](#)]
38. Nelson, R.A. Coordinate-dependent 3+1 formulation of the general relativity equations for a perfect fluid. *Gen. Relativ. Gravit.* **1981**, *13*, 569–580. [[CrossRef](#)]
39. Nelson, R.A. Post-Newtonian approximation for a rotating frame of reference. *Gen. Relativ. Gravit.* **1985**, *17*, 637–648. [[CrossRef](#)]
40. Nelson, R.A. Post-Newtonian approximation for an accelerated, rotating frame of reference. *Gen. Relativ. Gravit.* **1990**, *22*, 431–449. [[CrossRef](#)]
41. Chandrasekhar, S.; Nutku, Y. The second post-Newtonian equations of hydrodynamics in general relativity. *Astrophys. J.* **1990**, *5*, 86. [[CrossRef](#)]
42. Neves, J.C.S. Deforming regular black holes. *Int. J. Mod. Phys. A* **2017**, *32*, 1750112. [[CrossRef](#)]
43. Sharif, M.; Shahzadi, M. Neutral Particle Motion around a Schwarzschild Black Hole in Modified Gravity. *J. Exp. Theor. Phys.* **2018**, *127*, 491–502. [[CrossRef](#)]
44. Kolesnichenko, A.V. Constructing relativistic hydrodynamics of a simple fluid in a class of second-order theories. 2. The method of relativistic extended irreversible thermodynamics. *Prepr. Keldysh Inst. Appl. Math.* **2023**, *3*, 36. [[CrossRef](#)]
45. Eckart, A.; Hüttemann, A.; Kiefer, C.; Britzen, S.; Zajaček, M.; Lämmerzahl, C.; Stöckler, M.; Valencia-S, M.; Karas, V.; García-Marín, M. The Milky Way's Supermassive Black Hole: How Good a Case Is It? *Found. Phys.* **2017**, *47*, 553–624. [[CrossRef](#)]
46. Zhuravlev, V. Relativistic Standard Accretion Disc. In *Accretion Flows in Astrophysics*; Shakura, N., Ed.; Astrophysics and Space Science Library; Springer: Cham, Switzerland, 2018; Volume 454.
47. Abramowicz, M.A.; Fragile, P.C. Foundations of Black Hole Accretion Disk Theory. *Living Rev. Relativ.* **2013**, *16*, 1. [[CrossRef](#)] [[PubMed](#)]
48. Morse, P.M.; Feshbach, H. *Methods of Theoretical Physics, Part I*; McGraw-Hill: New York, NY, USA, 1953.

Disclaimer/Publisher's Note: The statements, opinions and data contained in all publications are solely those of the individual author(s) and contributor(s) and not of MDPI and/or the editor(s). MDPI and/or the editor(s) disclaim responsibility for any injury to people or property resulting from any ideas, methods, instructions or products referred to in the content.